# RESEARCH ARTICLE

Temozolomide Treatment Alters Mismatch Repair and Boosts Mutational Burden in Tumor and Blood of Colorectal Cancer Patients

Giovanni Crisafulli[1,2], Andrea Sartore-Bianchi[3,4], Luca Lazzari[5], Filippo Pietrantonio[6], Alessio Amatu[3], Marco Macagno[2], Ludovic Barault[1,2], Andrea Cassingena[3], Alice Bartolini[2], Paolo Luraghi[5], Gianluca Mauri[4,5], Paolo Battuello[1], Nicola Personeni[7,8], Maria Giulia Zampino[9], Valeria Pessei[2], Pietro Paolo Vitiello[1,2], Federica Tosi[3], Laura Idotta[3], Federica Morano[6], Emanuele Valtorta[3], Emanuela Bonoldi[3], Giovanni Germano[1,2], Federica Di Nicolantonio[1,2], Silvia Marsoni[5], Salvatore Siena[3,4], and Alberto Bardelli[1,2]
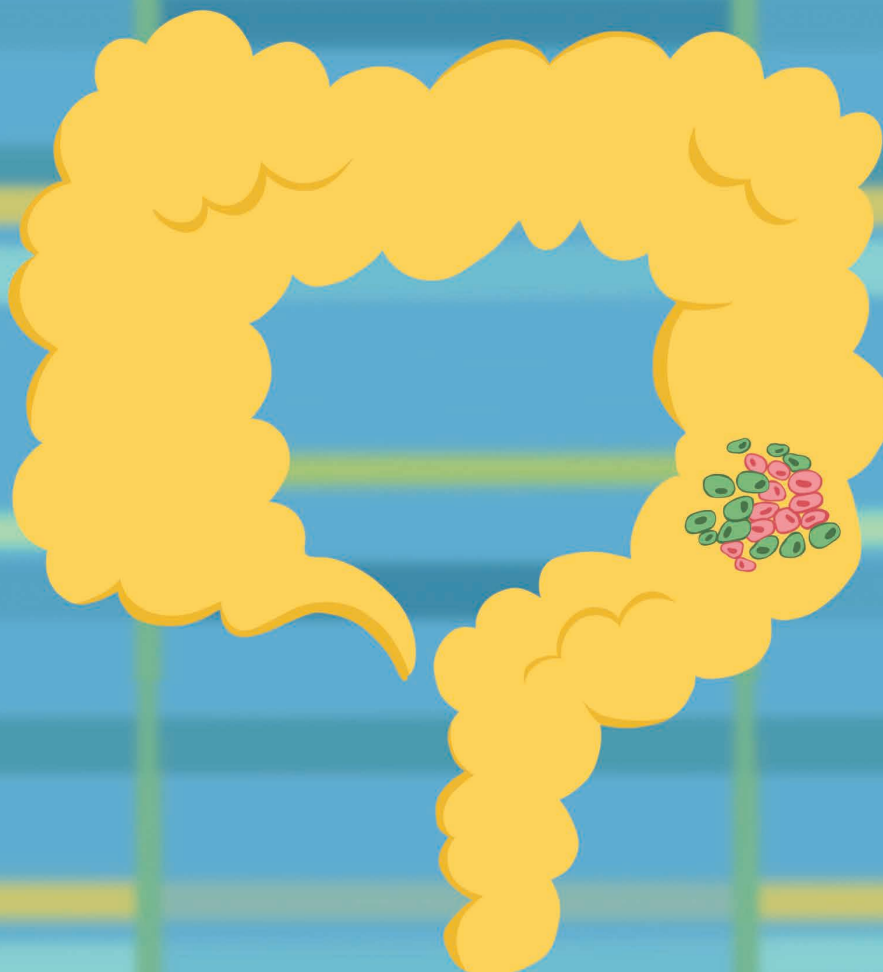
ABSTRACT

The majority of metastatic colorectal cancers (mCRC) are mismatch repair (MMR) proficient and unresponsive to immunotherapy, whereas MMR-deficient (MMRd) tumors often respond to immune-checkpoint blockade. We previously reported that the treatment of colorectal cancer preclinical models with temozolomide (TMZ) leads to MMR deficiency, increased tumor mutational burden (TMB), and sensitization to immunotherapy. To clinically translate these findings, we designed the ARETHUSA clinical trial whereby O6-methylguanine-DNA-methyltransferase (MGMT)–deficient, MMR-proficient, *RAS*-mutant mCRC patients received priming therapy with TMZ. Analysis of tissue biopsies and circulating tumor DNA (ctDNA) revealed the emergence of a distinct mutational signature and increased TMB after TMZ treatment. Multiple alterations in the nucleotide context favored by the TMZ signature emerged in MMR genes, and the p.T1219I *MSH6* variant was detected in ctDNA and tissue of 94% (16/17) of the cases. A subset of patients whose tumors displayed the *MSH6* mutation, the TMZ mutational signature, and increased TMB achieved disease stabilization upon pembrolizumab treatment.

SIGNIFICANCE: MMR-proficient mCRCs are unresponsive to immunotherapy. We provide the proof of concept that inactivation of MMR genes can be achieved pharmacologically with TMZ and molecularly monitored in the tissue and blood of patients with mCRC. This strategy deserves additional evaluation in mCRC patients whose tumors are no longer responsive to standard-of-care treatments.

See related commentary by Willis and Overman, p. 1612.

INTRODUCTION

Colorectal cancer is one of the most common and lethal cancers, representing around 10% of new cancer diagnoses and 9% of cancer-related deaths (1, 2). Although the 5-year relative overall survival rate ranges between 68% and 90% in localized disease (stages I–III), the rate in stage IV metastatic colorectal cancer (mCRC) is still dismal, dropping to between 11% and 14% (1, 2).

Cytotoxic combinations represent the main therapeutic options for most mCRC patients (3, 4). Despite recent progress

exploiting targeted therapies such as a combination of BRAF and EGFR inhibitors for *BRAF*[V600E]-mutant tumors or HER2 blockade in HER2-positive ones, treatment developments have been incremental rather than transformative (5–9).

The mismatch repair (MMR) system, which detects and corrects base mispairs as well as insertions and deletions (indels) that occur during DNA synthesis, is deregulated in approximately 15% of stage I to III colorectal cancers and 5% of mCRC (10, 11). Based on the MMR proficiency status, colorectal cancers are classified into two molecularly distinct subgroups defined as mismatch repair–proficient (MMRp) or mismatch repair–deficient (MMRd; refs. 12, 13). MMRp tumors include those that are usually microsatellite stable (MSS) or tumors with intact MMR proteins, accounting for around 95% of mCRCs (14). MMRd tumors usually present microsatellite instability (MSI) as a consequence of genetic or epigenetic alterations leading to the inactivation of MMR genes, such as *MLH1*, *MSH2*, *MSH6*, and *PMS2* (15). As a result of defective MMR machinery, MMRd tumor cells display a high number of genomic alterations leading to the production of non–self-peptides, which should be recognized by the immune system (16, 17). This hypothesis is consistent with the observation that MSI/MMRd colorectal cancers are counterselected during progression toward metastatic disease and display an overall better prognosis with respect to the MSS/MMRp counterpart (18). Immune therapy based on anti–programmed death-1 (PD-1) agents is highly effective in patients with MSI/MMRd mCRC. In the first line, the anti–PD-1 agent pembrolizumab led to superior progression-free survival (PFS) compared with chemotherapy for MSI/MMRd mCRC (19). In the same setting, a single-arm phase II trial also found that the combination of another anti–PD-1, nivolumab, plus a low dose of the anti–cytotoxic T-lymphocyte antigen 4 (CTLA4) ipilimumab demonstrated an extremely high rate of durable clinical

[1]Department of Oncology, University of Torino, Candiolo, Italy. [2]Candiolo Cancer Institute, FPO - IRCCS, Candiolo, Italy. [3]Niguarda Cancer Center, Grande Ospedale Metropolitano Niguarda, Milan, Italy. [4]Department of Oncology and Hemato-Oncology, Università degli Studi di Milano, Milan, Italy. [5]The FIRC Institute of Molecular Oncology, Milan, Italy. [6]Department of Medical Oncology, Fondazione IRCCS Istituto Nazionale dei Tumori, Milan, Italy. [7]Department of Biomedical Sciences, Humanitas University, Pieve Emanuele, Milan, Italy. [8]Medical Oncology and Hematology Unit, Humanitas Cancer Center, IRCCS Humanitas Research Hospital, Rozzano, Milan, Italy. [9]Division of Gastrointestinal Medical Oncology and Neuroendocrine Tumors, European Institute of Oncology, IRCCS, Milan, Italy.

Note: Supplementary data for this article are available at Cancer Discovery Online (http://cancerdiscovery.aacrjournals.org/).

G. Crisafulli, A. Sartore-Bianchi, and L. Lazzari contributed equally to this article.

F. Di Nicolantonio, S. Marsoni, S. Siena, and A. Bardelli are co–senior authors of this article.

Corresponding Author: Alberto Bardelli, University of Turin, Department of Oncology, Candiolo Cancer Institute, FPO - IRCCS, Str.Prov.le 142, km 3.95, 10060, Candiolo, Torino, Italy. Phone/Fax: 39-011-993-3235; E-mail: alberto.bardelli@unito.it

American Association for Cancer Research

benefit (20). The latter combination is now being tested in a confirmatory randomized phase III trial versus nivolumab alone or physician's choice chemotherapy (CheckMate 8HW trial, NCT04008030). In patients with chemorefractory disease, results from phase II trials with pembrolizumab (21) or the combination of nivolumab and ipilimumab (22) have also shown promising efficacy in terms of response rate and PFS, providing the grounds for escalation to first line. As a whole, these results are radically transforming treatment guidelines and affect real-world MSI/MMRd mCRC patients (23).

A rare subset of MSS mCRCs harboring mutations in the exonuclease domain of DNA polymerase epsilon (*POLE*) gene display an ultramutated phenotype with a significantly higher tumor mutational burden (TMB) than MSI/MMRd CRCs. *POLE*-mutant MSS tumors are characterized by a high number of single-nucleotide variants (SNV) and have also been found to be exquisitely sensitive to immune checkpoint blockade (ICB; refs. 14, 24). Interestingly, both MSI carrying elevated levels of indels/frameshifts and *POLE*-mutant colorectal cancer (characterized by elevated SNVs and much fewer indels/frameshifts) benefit from immunotherapy. This indicates that both classes of genetic alterations can trigger an immune response.

Although ICB dramatically affected the prognosis of patients with MSI/MMRd and MSS *POLE*-mutant mCRC, MSS/MMRp mCRCs are intrinsically resistant to anti–PD-1–based regimens (25). Indeed, MSS/MMRp mCRCs are characterized by low TMB, an immune-suppressive tumor microenvironment with a low level of tumor-infiltrating lymphocytes, and reduced expression of checkpoint proteins (17). Thus, MSS/MMRp mCRCs are usually defined as "cold," as opposed to their "immunologically hot" MSI/MMRd counterpart (17). One of the current greatest challenges for translational research in mCRC is to understand how to switch immunologically cold tumors into hot tumors.

Different combinations of checkpoint inhibitors with cytotoxic, anti–vascular endothelial growth factor (anti-VEGF), anti-EGFR agents, or tyrosine kinase inhibitors have been tested in clinical trials in MSS/MMRp mCRCs, but overall results remain disappointingly inconclusive (14, 26–30).

The alkylating agent temozolomide (TMZ) is a treatment option in several solid tumors such as glioma, glioblastoma, neuroendocrine tumors, melanoma, and sarcomas (31–37). Resistance to TMZ in O6-methylguanine-DNA-methyltransferase (*MGMT*)–methylated glioblastomas is associated with the onset of inactivating mutations in MMR genes, such as *MSH6* (38–41). Recurrent tumors are more frequently hypermutated, which may potentially sensitize glioblastomas to ICB (42, 43). This observation led to currently ongoing phase II trials assessing the effectiveness of ICB in recurrent hypermutated glioma and glioblastoma (NCT04145115 and NCT02658279).

Using a syngeneic colorectal cancer mouse model, our group previously demonstrated that TMZ treatment led to the emergence of MMRd cells among an otherwise MMRp cell population (44). Interestingly, these cells were more immunogenic and triggered immune surveillance in mice (44). Additionally, analysis of tumor biopsies from mCRC patients relapsing after TMZ-based therapeutic regimens revealed MMR mutations as a potential resistance mechanism in two out of five cases (44). Finally, our data suggested

that MMR inactivation in mouse and human CRCs could lead to increased TMB and predicted neoantigens (44). These data led to the design of ARETHUSA (NCT03519412), an ongoing proof-of-concept, two-step clinical trial. During the first step—the priming phase—TMZ treatment is used both with therapeutic intent and to trigger a hypermutant status in patients with *MGMT*-hypermethylated MSS mCRC. In the second step—the immunotherapy phase—the anti–PD-1 agent pembrolizumab is deployed as monotherapy in those patients who develop a TMB ≥20 mutations per megabase (mut/Mb) upon progression after TMZ treatment.

Here we present the analyses of tissue biopsies and circulating tumor DNA (ctDNA) obtained from an initial cohort of 21 ARETHUSA patients before and after the priming phase. We provide clinical proof of concept that targeting DNA repair processes can affect the mutational evolution of MSS/MMRp tumors and be potentially exploited as a noncanonical strategy to turn immunologically cold tumors into hot tumors.

RESULTS

Clinical Flow and Logistics of the ARETHUSA Trial

We selected *RAS*-mutated mCRC patients who had progressive disease (PD) on or after prior systemic treatment including fluoropyrimidines, oxaliplatin, irinotecan, regorafenib, or trifluridine/tipiracil. All patients were screened for MMR and/or MSI status on archival formalin-fixed, paraffin-embedded tumor tissues.

The status of the *MGMT* gene and protein was evaluated during the screening phase before enrolling the patient in the priming phase. To enter this phase, eligible patients must have had tumors (i) with no or low expression of MGMT protein as defined by a negative IHC staining and (ii) with hypermethylation at the *MGMT* gene promoter level as defined by a positive methyl-BEAMing analysis. These were mandatory criteria for the molecular screening of patients before enrollment. We previously demonstrated that *MGMT*-methylated mCRCs are more likely to benefit from TMZ than those lacking *MGMT* methylation (45–49). Accordingly, TMZ priming was restricted to patients with MGMT-defective tumors assessed by both protein expression and promoter methylation because this two-layer selection has been identified as the most effective by a large pooled cohort in this setting (49). Patients were also biopsied before (nonmandatory) and after (mandatory) TMZ treatment to determine the post-TMZ TMB and whenever possible any changes in TMB over time (Fig. 1). A post-TMZ threshold of 20 mut/Mb [i.e., double that required for the standard-of-care (SOC) use of the anti–PD-1 antibody pembrolizumab; refs. 15, 50] was required to access the immunotherapy phase delivering pembrolizumab every 3 weeks until PD or unacceptable toxicity (Fig. 1). The ARETHUSA clinical trial is currently ongoing and recruiting patients with mCRC (NCT03519412), whereas the translational analyses of an initial cohort of 21 patients enrolled in the trial are presented here.

Clinical Efficacy of TMZ in the Priming Phase of the ARETHUSA Trial

From February 2019 to December 2021 (data lock for the present study), 473 MSS/MMRp, *RAS*-mutant mCRC
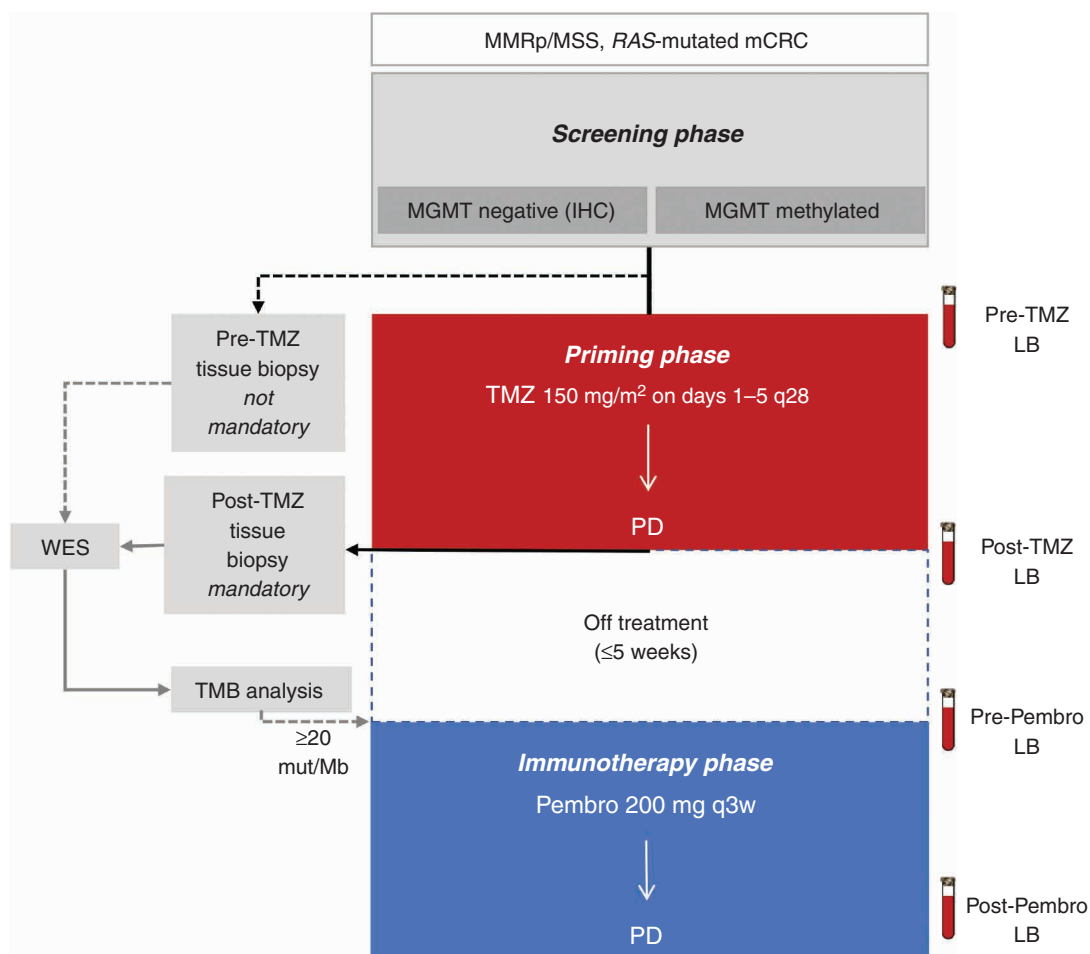
Figure 1. The ARETHUSA trial. Graphical description of the ARETHUSA trial. MGMT-deficient, *RAS*-mutant, and MMRp mCRC patients received priming therapy with TMZ. A post-TMZ TMB threshold of 20 mutations/Mb was required to access the immunotherapy phase delivering pembrolizumab every 3 weeks. IHC, immunohistochemistry; LB, liquid biopsy; MB, methyl-BEAMing; q28, every 28 days; q3w, every 3 weeks; Pembro, pembrolizumab; WES, whole exome sequencing.

patients were enrolled in the study; 442 patients were screened for MGMT status and 33 of 69 *MGMT*-methylated patients received priming treatment with TMZ. Twenty-seven patients were treated with TMZ until PD, whereas treatment of six patients was currently ongoing at the time of data lock. We included in ARETHUSA three additional patients who had PD on TMZ-based regimens as part of other trials (51, 52) or on TMZ off-label treatment (Supplementary Fig. S1). Of the 30 patients treated in the priming phase until PD, TMZ was administered for a median of 3 months of treatment (range, 0.6–7.5; Fig. 2). TMZ priming achieved a disease control rate (DCR) of 57% [17/30, 57%; 95% confidence interval (CI), 39%–74%]. Unsurprisingly, in a heavily pretreated *RAS*-mutant patient population such as in ARETHUSA [median prior regimen *n* = 3 (range, 1–6); 63% (19/30) of patients with previous ≥3 therapeutic lines], DCR consisted of disease stabilization (SD) as RECIST 1.1 best response, with a median PFS of 4.2 months (range, 2.7–7.5; Fig. 2). However, tumor growth stabilization lasting ≥4 months (corresponding to at least 5 cycles of TMZ) was achieved in 10 of 17 patients (10/17, 59%; 95% CI,

35%–82%). The median PFS in patients experiencing PD as best response was 2.0 months (range, 0.6–2.4; Fig. 2). A post-TMZ biopsy was performed in 21 patients at PD (Fig. 2; Supplementary Fig. S1; Supplementary Table S1). Biopsy at PD was not performed in nine cases due to the deteriorating clinical conditions of patients (Fig. 2).

TMZ was tolerated as expected in this setting, without drug-related serious adverse events (SAE) except for hematologic (neutropenia/thrombocytopenia; *n* = 1) and gastrointestinal (*n* = 1) toxicities, consistent with previous studies (45, 47). Particularly, neither death nor life-threatening SAEs have been reported. In summary, TMZ priming can be safely delivered as a third-/fourth-line treatment in patients with *MGMT*-hypermethylated, *RAS*-mutated mCRC and tissue biopsies can be obtained at PD in most patients.

Identification of the TMZ Signature in Colorectal Cancer Cells Treated with TMZ

Somatic mutations are caused by distinct mutational processes, generating characteristic mutational signatures that can be detected in the genome of cancer cells (53–56).
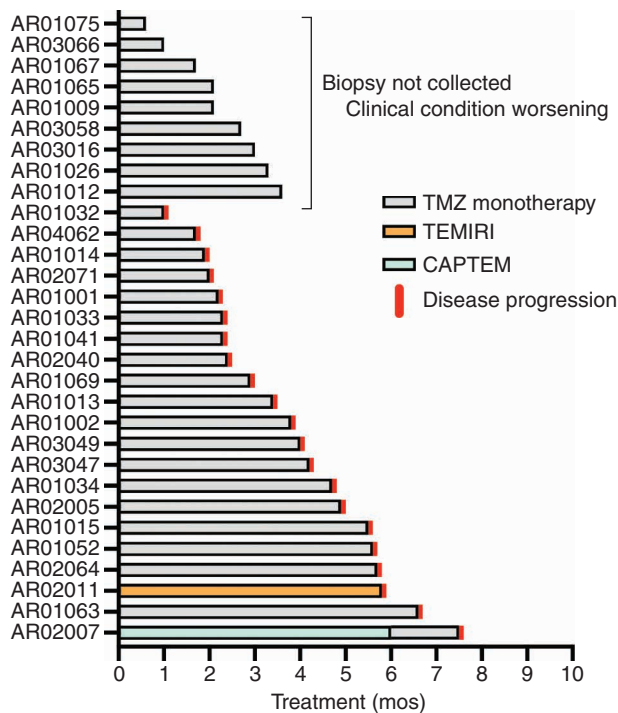
Figure 2. Clinical response to TMZ in ARETHUSA patients. Swimmer plot of clinical time on treatment in the TMZ priming phase: 27 patients were treated with TMZ monotherapy until clinical or radiologic (based on RECIST 1.1 criteria) disease progression. Three patients AR02005, AR02007, and AR02011 were treated with TMZ-based regimens and enrolled in ARETHUSA according to protocol violation. Post-TMZ tissues for TMB evaluation were collected in 21 patients; 9 cases were excluded due to the clinical condition worsening. CAPTEM, capecitabine + TMZ combination; mos, months of treatment; TEMIRI, TMZ + irinotecan combination.

The analysis of mutational signatures using the "fitting" method involves a sequence of mathematical steps designed to identify the best known signatures (or a combination of thereof) that can explain the observed mutational profile in an individual sample (57). Many of these signatures have been associated with a defined etiology, including exposure to a specific treatment, known carcinogens, and defective or error-prone DNA repair proteins (53, 54, 58). Notably, previous works have shown that mutational signature analyses can readily identify the effect of alkylating agents such as TMZ (53, 54, 58). In particular, mutational signature 11 [single base substitution 11 (SBS11)] was found in patients

with malignant melanoma or glioblastoma and was previously reported in experimental studies with alkylating agents (53, 54, 58). We reasoned that mutational signature assessment in tissue samples collected at the end of the priming phase could help to mechanistically determine the molecular impact and the functional implications of TMZ treatment and predict the efficacy of subsequent immunotherapies in ARETHUSA patients.

To assess the specificity of signature profile identification, we examined whole exome sequencing (WES) data from a panel of 12 cell lines, including MSS, MSI, and *POLE*-mutated models. As shown in Supplementary Fig. S2A, signature 1 (age related) was readily identified in all cell lines, whereas signatures 6/15/26 (associated with MMR deficiency) and signature 10 (related to *POLE* mutations) were detected in MMRd/MSI and *POLE*-mutated cell models, respectively (Supplementary Fig. S2A). Next, as a positive control to demonstrate the proper identification of the TMZ signature in the colorectal cancer genome, we treated two *MGMT*-methylated colorectal cancer cell models (SKCO1 and SW620) with TMZ, as previously reported (44). For both parental and TMZ-treated cells, genetic analyses were performed to systematically detect mutational signatures. As expected, the alkylating agent–related signature 11 was evident only in colorectal cancer cells treated with TMZ, confirming the specificity of the approach (Supplementary Fig. S2B).

Detection of the TMZ Signature in Tumor Biopsies after Treatment with TMZ

Upon validation in cell models, the approach was then used to identify mutational signatures using WES data of post-TMZ tumor samples collected from all 21 biopsied patients (Supplementary Table S1; Supplementary Fig. S1). Tumor biopsies obtained at TMZ progression were analyzed to evaluate TMB and establish the eligibility to pembrolizumab treatment (Fig. 1). TMB analysis was also performed on samples from five patients with an available pre-TMZ tissue biopsy (Fig. 1). Mutation calling was initially performed using a threshold variant allelic frequency (VAF) value ≥10% to select molecular alterations occurring in a predominantly clonal fashion (as reported in ref. 15). Using this approach, two patients (AR02007 and AR01052) scored positive for the alkylating agent–related signature 11 (Fig. 3A). In these two cases, 78% and 77% of the mutations, respectively, could be attributed to TMZ treatment (Fig. 3A).

We reasoned that, as for other anticancer therapies, molecular changes triggered by TMZ treatment were likely

Figure 3. Mutational signature and TMB analysis in biopsies after TMZ treatment. **A** and **B,** Mutational signature analysis measuring the impact of TMZ priming on tissue biopsies assessed by next-generation sequencing. Patients were classified in three subtypes—A, B1, and B2—based on the score of the mutational signature 11 and TMB value. In **A,** only clonal mutations (adjusted fractional abundance ≥10%) were used to generate the heat map. In five cases (AR02071, AR01032, AR01014, AR01069, and AR02064), the number of mutations was not sufficient to properly perform mutational analysis (cosine similarity lower than 0.9) and these five samples were excluded. In **B,** all mutations (adjusted fractional abundance ≥1%) were considered for heat map generation. **C,** TMB expressed as mut/Mb after the priming phase for the three groups of patients. The relative contribution of clonal (yellow) and subclonal (blue) alterations to TMB is listed for each patient. Inset, positive linear correlation between mutations induced by signature 11 (TMZ) normalized for megabases and TMZ cycles of treatment. Spearman rank correlation is listed ($P = 2.535e{-}5$ and $R = 0.7847$). **D,** TMB expressed as mut/Mb after the priming phase for the three groups of patients. The relative contribution of SNVs and indels to TMB is listed for each patient. **E,** The best response to TMZ treatment is also reported for each patient. Subtype A (yellow): patients with no molecular evidence of TMZ treatment. Subtype B1 (blue): patients with subclonal molecular evidence of TMZ treatment. Subtype B2 (green): patients with clonal molecular evidence of TMZ treatment. Sig, signature.
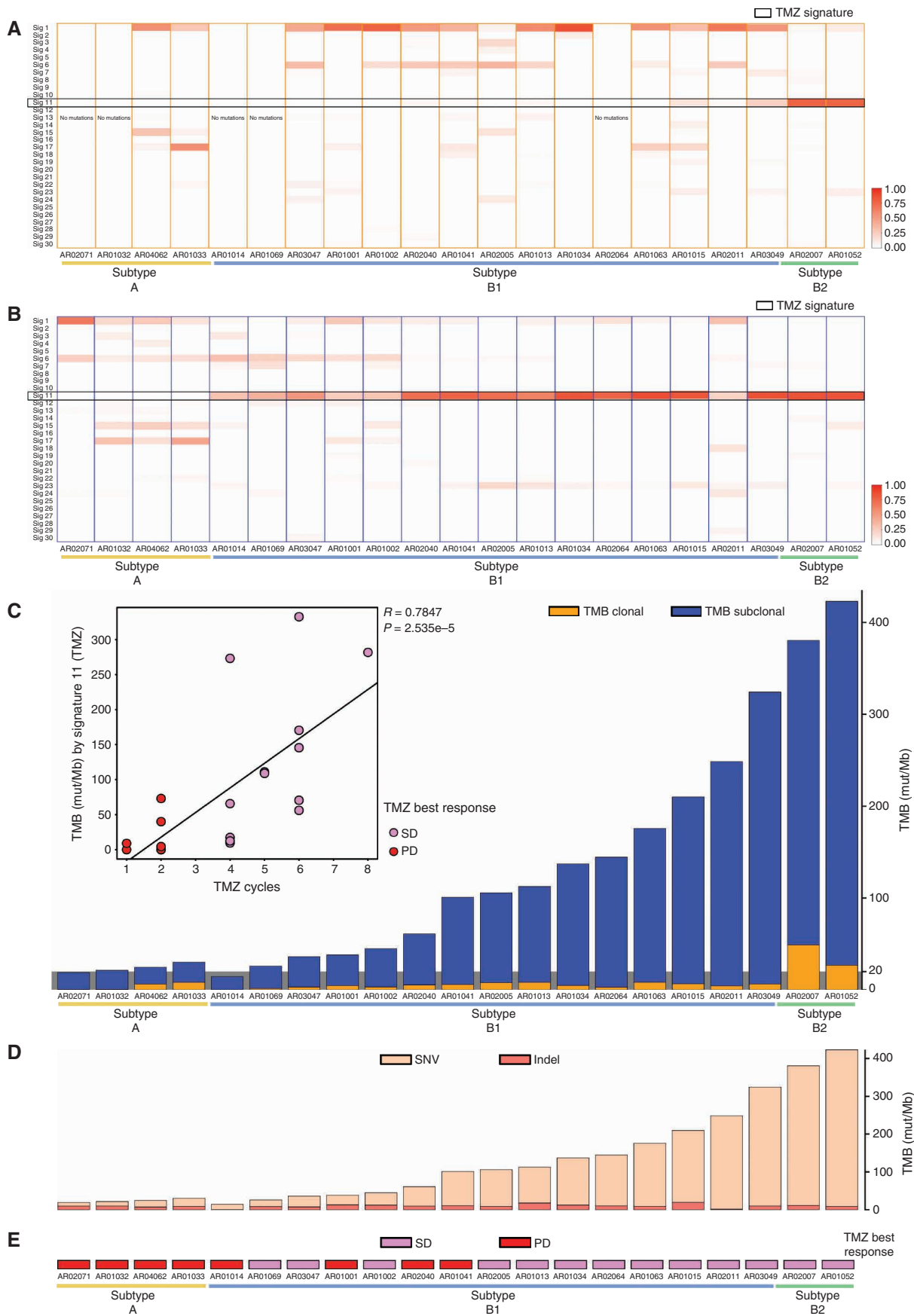
to occur at subclonal levels and in a heterogeneous manner. To evaluate this possibility, we performed mutational signature analysis also considering somatic variants with VAF <10% (subclonal analysis). This was feasible considering that we sequenced high-quality DNA obtained from fresh tissues and used a high-depth sequencing approach (median depth 376× with PhredScore ≥30 and coverage ≥96.82% at 100× depth) that gathered a median of 124 million reads per sample (Supplementary Table S1).

Using clonal and subclonal combined TMZ mutational profiling, we found that colorectal cancer samples from ARETHUSA patients could be classified into two main categories: subtypes A and B. Subtype A ($n = 4$) encompasses tumor samples scoring negative for signature 11 and includes patients who received a few TMZ cycles (Fig. 3A and B; Supplementary Table S2). On the other hand, subtype B ($n = 17$) features tissue samples collected from patients who received longer TMZ treatment and in which signature 11 can be identified (Fig. 3A and B; Supplementary Table S2). Notably, according to the clonality score of the variants used to detect signature 11, subtype B could be further subdivided into two subclasses (Fig. 3A and B): subtype B1, including all those tumor samples in which signature 11 is detected at the subclonal level ($n = 15$), and subtype B2, in which the presence of signature 11 is defined at the clonal level ($n = 2$).

Although in subtype B1, only a fraction of the cells evaluated in the biopsy are affected by TMZ treatment and acquire signature 11, in subtype B2 a larger fraction of the tumor cells display the characteristic molecular imprint of TMZ treatment (Fig. 3A and B). In five cases (AR02071, AR01032, AR01014, AR01069, and AR02064), the number of mutations was not sufficient to properly perform mutational analysis of clonal variants, and these samples were excluded from the analysis (cosine similarity lower than 0.9; see Supplementary Fig. S2C and D and the Methods section for details).

To exclude that patient stratification in subtypes A, B1, and B2 could be affected by the reference signatures that were used for the mutational analysis fitting, we performed clonal and subclonal scrutiny using three reference signature databases available in COSMIC (v 2.0, v 3.0, and v 3.2) and two distinct bioinformatic tools (see Methods for details). These analyses led to comparable results (Fig. 3A and B; Supplementary Fig. S3A and S3B).

To evaluate how patient stratification was affected by the heterogeneity of the tumor biopsy, we checked the performance of the clonal/subclonal analysis comparing the reconstructed mutational profile (after fitting) with the original mutational profile of the sample using the cosine similarity as a parameter (59, 60). The cosine similarity parameter quantifies two-vector similarities and spans from 1 (identical) to 0 (distinct). A high cosine similarity value (closer to 1) indicates suitable reconstruction of the processes determining mutation accumulation (59, 60). We found that cosine similarity was always higher than 0.90 and 0.95 in the clonal and subclonal analyses, respectively (Supplementary Fig. S2C and S2D). In summary, this observation supports the validity of the results obtained in the subclonal analysis, suggesting that it can confidently capture the relative contribution of each mutational signature (including the TMZ effect) and

classify tumor samples based on the etiologic origin of their mutations (Supplementary Fig. S2C and S2D).

## Assessment of TMB in Tissue Biopsies after TMZ Priming

TMB was calculated on the high-depth WES of tumor tissue biopsies using peripheral blood mononuclear cells (PBMC) as a normal matched sample (Supplementary Table S1). We applied the same workflow used for the mutational signature analyses initially considering mutations with VAF ≥10%. Based on this cutoff, patients AR02007 and AR01052 displayed 49 mut/Mb and 27 mut/Mb, respectively (Fig. 3C), whereas all other cases displayed less than 10 mut/Mb (Fig. 3C), a value commonly found in MSS colorectal cancers (15). Interestingly, only the two patients with TMB ≥20 mut/Mb (AR02007 and AR01052) also displayed a high clonal score for signature 11 (Fig. 3A), whereas the remaining patients had a low clonal TMB (<10 mut/Mb) and a low signature 11 score in post-TMZ biopsies (Fig. 3A and C).

The availability of high-depth next-generation sequencing (NGS) data (median depth 376× with PhredScore ≥30 and coverage ≥96.82% at 100× depth; Supplementary Table S1) also allowed TMB assessment at the subclonal level (considering mutations with VAF <10%). Samples from subtype A mCRC had an average subclonal TMB post-TMZ of 24 mut/Mb, whereas samples from subtype B had a higher average subclonal TMB post-TMZ of 152 mut/Mb ($P < 0.0007$; Fig. 3C).

We also evaluated the contribution of SNVs and indels to TMB (Fig. 3D). Notably, a prominent impact of TMZ on the tumors (from left to right in Fig. 3) was paralleled by an increase of SNVs, whereas the absolute number of indels remained similar in all tumors. This is in line with previous reports from our group and others (44, 53, 54).

Next, we studied whether and to what extent the number of TMZ cycles affected the molecular profiles of post-TMZ biopsies. We noted that patients with subtype B mCRC and higher subclonal TMB had disease control (SD) with longer TMZ treatment as compared with patients with subtype A mCRC, who experienced PD as the best response without benefiting from TMZ, thus receiving lower drug exposure (Fig. 3C–E; Supplementary Table S2). Notably, a linear positive correlation between the number of mut/Mb induced by TMZ signature and cycles of TMZ treatment in patients was observed (Spearman rank correlation, $R = 0.7847$, $P = 2.535e-5$; Pearson $R = 0.6887$, $P = 0.00055$; inset of Fig. 3C). This strongly suggests that molecular differences occurring in subtype B1/B2 could be attributed to the level of exposure to TMZ.

Although a post-TMZ biopsy was mandatory for all ARETHUSA patients, an exploratory pre-TMZ biopsy was also performed in 5 of 21 patients (4 subtype B, 1 subtype A). These valuable samples allowed us to comparatively study the impact of TMZ on mutational signatures and TMB (Fig. 4A–C). In these cases, a comparison between matched pre– and post–TMZ treatment biopsies confirmed that SBS11 was absent in all samples obtained before TMZ treatment in both patients with subtype A (Fig. 4A) and subtype B1 (Fig. 4B). These analyses further corroborated the emergence of signature 11 post-TMZ in patients with subtype B1 (Fig. 4B) and revealed that the increase of TMB was the highest in subtype B1 tumors (Fig. 4C).
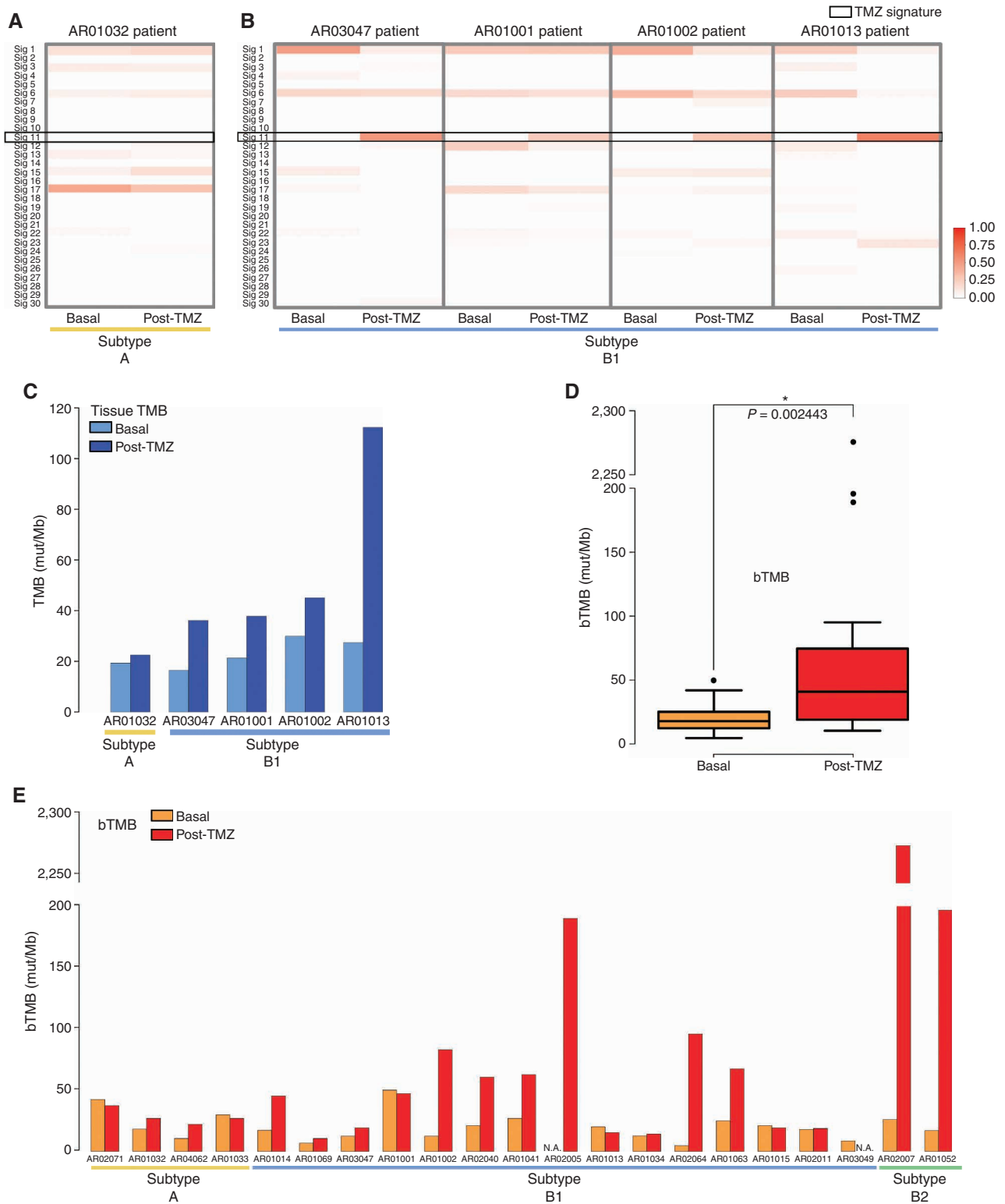
Figure 4. Comparison of signature and TMB analysis of tissue/blood samples before and after TMZ priming. **A,** Signature contribution before and after TMZ priming in tissue samples of subtype A patients. **B,** Signature contribution before and after TMZ priming in tissue samples of subtype B patients. **C,** TMB in tumor tissue before and after TMZ priming. **D** and **E,** bTMB expressed as mut/Mb before and after the TMZ priming phase in aggregate (**D**) and in detail for each patient (**E**). Wilcoxon rank-sum test, $P = 0.002443$. Subtype A (yellow): patients with no genetic evidence of TMZ treatment. Subtype B1 (blue): patients with subclonal genetic evidence of TMZ treatment. Subtype B2 (green): patients with clonal genetic evidence of TMZ treatment. Basal, analysis of tumor before priming phase of the ARETHUSA trial; post-TMZ, analysis of tumor after priming phase of ARETHUSA trial; N.A., not available; Sig, signature.

Assessment of TMB in Blood before and after TMZ Priming

Considering that tissue biopsies often represent only a spatial–temporal snapshot of the tumor genomic heterogeneity and that we detected molecular heterogeneity post-TMZ (subtypes A, B1, and B2), we also studied ctDNA, as this approach may more comprehensively capture the whole molecular profile of metastatic tumor (61, 62) and more easily integrate into the therapeutic path of patients than a tissue biopsy. Conveniently, we had collected longitudinal blood samples including pre- and post–TMZ treatment for most patients (Fig. 1). Blood TMB (bTMB) was measured in plasma samples before and after TMZ treatment (Fig. 1) using a validated assay for tissue/blood correlative analyses (63).

The median bTMB value evaluated in basal plasma samples was 18.18 mut/Mb (Fig. 4D). A comparison of bTMB in matched pre–post-TMZ plasma samples allowed us to conclude that in most patients, high TMB values assessed in tissue were indeed induced by TMZ and that the ARETHUSA priming phase significantly increases bTMB ($P = 0.002443$, Wilcoxon rank-sum test; Fig. 4D and E).

Collectively, bTMB values were comparable with those of subclonal TMB calculated by WES on tissue biopsies (Figs. 3C and 4E) except for patients with lesions localized mainly in the lung and/or peritoneum. In fact, different from cases carrying predominantly liver lesions, the maximum VAF detected in both pre- and post-TMZ blood samples in these patients (AR02011, AR01015, and AR01034) was below 10%, thus affecting bTMB (Supplementary Table S2). This is likely related to the impact of metastatic sites on ctDNA release capacity and detection, as recently reported (64). Interestingly, the two subtype B2 patients (AR02007 and AR01052, subtype B2 with clonal TMZ signature; Fig. 3C) showed a bTMB value of 2,276 and 196 mut/Mb, respectively (AR02007 and AR01052, subtype B2; Fig. 4E).

Mutations in MMR Genes in Post–TMZ Treatment Biopsies

We and others have shown that secondary resistance to anticancer therapies is associated with changes in the tumor mutational profiles, including the emergence of mutations in key effectors of the pathway targeted by the anticancer drug (65, 66).

Current knowledge on the resistance mechanisms to TMZ has been obtained studying glioma and glioblastoma (39), and we were the first to report how secondary resistance to TMZ in colorectal cancer preclinical models selects tumor cells carrying alterations in other genes involved in the DNA MMR system, such as *MHL1* or *MSH6* (44). Those findings laid the preclinical rationale of the ARETHUSA design that is aimed at therapeutically exploiting the mutations induced by TMZ treatment. To this end, we used an integrated bioinformatic pipeline to assess SNVs, indels, and gene copy-number alterations starting from WES data

(67, 68). By comparing somatic alterations that emerged in tissue samples post-TMZ, we identified a list of recurrently mutated genes. Interestingly, *MSH6* gene mutations recur upon treatment in multiple patients (8/17, 47% subtype B tumors). In particular, three *MSH6* mutations (p.T1219I, p.G557D, and p.G1139S) were present in six ARETHUSA subtype B tissue samples but not in subtype A samples (Supplementary Table S3). Functionally, these mutations have been found to decrease the efficiency of MMR machinery, as determined by *in vitro* assays (69).

Recurrent *MSH6* Mutations in mCRC Treated with TMZ

Plasma samples collected at pre- and post-TMZ time points were analyzed to evaluate the genetic profile of MMR genes. Mutational profiles of ctDNA revealed again two main categories of patients, confirming the previous stratification based on subclonal signature analysis. The *MSH6* gene alterations were not detected in plasma/tissue samples of subtype A cases, but, strikingly, they were found in 17 of 17 (100%) of subtype B cases, with a high prevalence of the *MSH6* p.T1219I variant (16/17, 94%). Importantly, it was never detected in the 5 tissue biopsies and all 20 plasma pre-TMZ samples available for the analysis (Supplementary Table S3). Overall, these results indicate that in colorectal cancer, the p.T1219I *MSH6* mutation emerges at a very high frequency (94%) as a molecular response marker to extended exposure to TMZ. Given that the p.T1219I variant was never identified in subtype A cases (who also received TMZ), the occurrence of this variant does not simply reflect exposure to TMZ, but is also indicative of both molecular (TMB increase) and clinical (tumor response/ stabilization) effects of TMZ treatment. Furthermore, the *MSH6* variant was exclusively detected in patients positive for signature 11 (subclonal score >0, subtype B tumors; Supplementary Table S3).

Based on these findings, we formulated the hypothesis that the recurrent *MSH6* mutation was related to the TMZ mutational signature. To test this possibility, we checked whether the genomic region encoding the p.T1219I variant lies in the nucleotide context favored by signature 11 and indeed found that this was the case (Fig. 5A and B). To exclude that the *MSH6* gene was enriched in nucleotide contexts favored by the emergence of mutational signature 11 (triplets mutated with high probability), we compared the sequence context of the *APC* gene (which served as control) and other MMR genes (Supplementary Fig. S4A). The analysis revealed the absence of biases toward the *MSH6* sequence as compared with other MMR genes (Supplementary Fig. S4A). Next, we reanalyzed tissue and ctDNA mutational profiles for additional variants and found that *MSH6* mutations could be detected in both tissue and matched ctDNA only when obtained after TMZ. Notably, virtually all (100%) of these SNVs were always causally linked to signature 11 (Supplementary Table S3; Fig. 4A and B; Supplementary Fig. S4B).

Figure 5. *MSH6* genetic alterations in ARETHUSA patients and their genetic context. **A,** Mutation type probability according to signature 11 and *MSH6* mutations emerged after TMZ treatment. The contexts of each mutation in the *MSH6* gene in both tissue biopsy and blood post-TMZ priming are shown; mutations that are likely to inactivate MMR are reported in bold. **B,** *MSH6* genetic alterations identified in tissue and blood after TMZ priming. Mutations potentially affecting the MMR status (MMRp to MMRd) are listed in bold. dMMR, deficient mismatch repair.
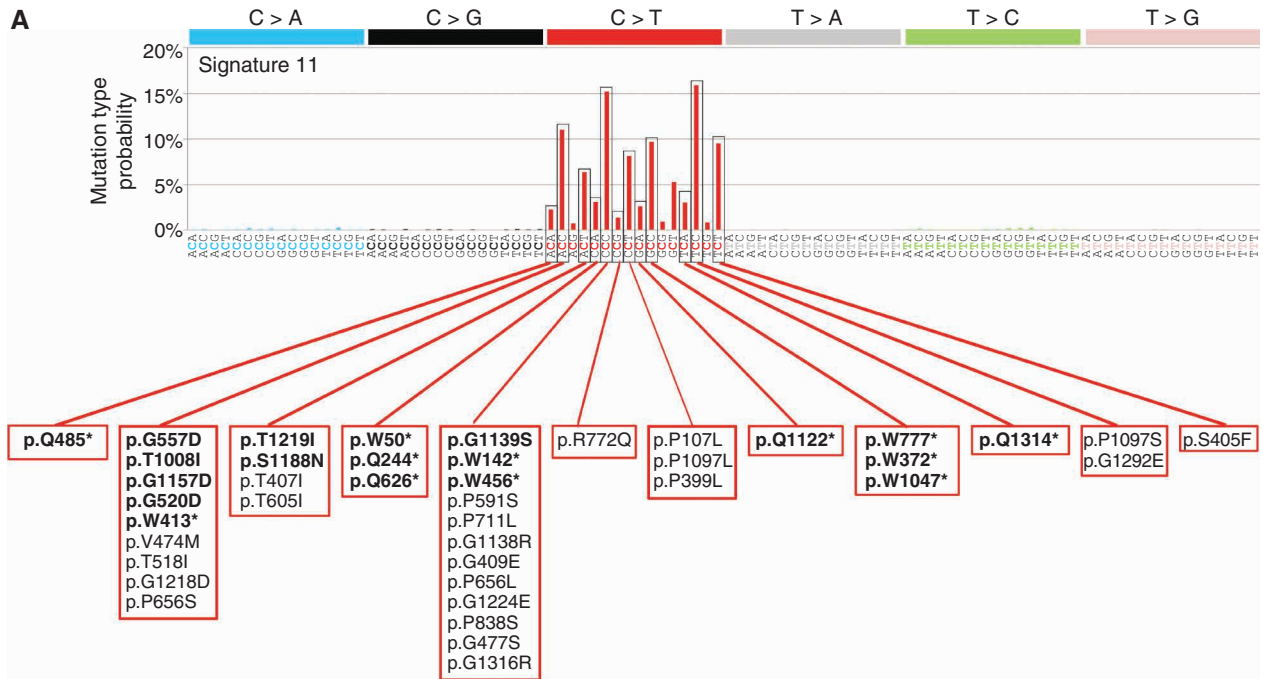
B

MSH6 alteration	Coord	Patient	Patient_ID	dMMR status
p.T1219I	chr2:48033352	16	AR01014; AR01001; AR01002; AR02005; AR010013; AR01015; AR01034; AR01041; AR02040; AR02011; AR02007; AR03049; AR01052; AR01063; AR02064; AR03047	Drost et al., 2020
p.G557D	chr2:48026792	2	AR01034; AR02005	Drost et al., 2020
p.T1008I	chr2:48028145	2	AR02005; AR01052	Drost et al., 2020
p.Q1122*	chr2:48030750	2	AR02007; AR02064	STOP codon acquisition
p.W777*	chr2:48027453	1	AR01034	STOP codon acquisition
p.W50*	chr2:48010521	1	AR01034	STOP codon acquisition
p.G1139S	chr2:48030801	1	AR02007	Drost et al., 2020
p.W142*	chr2:48018231	1	AR02007	STOP codon acquisition
p.Q1314*	chr2:48033729	1	AR02007	STOP codon acquisition
p.W372*	chr2:48026238	1	AR02007	STOP codon acquisition
p.Q244*	chr2:48025852	1	AR02007	STOP codon acquisition
p.G1157D	chr2:48032080	1	AR02005	Drost et al., 2020
p.G520D	chr2:48026681	1	AR02005	Drost et al., 2020
p.W413*	chr2:48026361	1	AR02005	STOP codon acquisition
p.W456*	chr2:48026490	1	AR02005	STOP codon acquisition
p.Q626*	chr2:48026998	1	AR02005	STOP codon acquisition
p.W1047*	chr2:48028263	1	AR01063	STOP codon acquisition
p.S1188N	chr2:48032763	1	AR01063	Drost et al., 2020
p.Q485*	chr2:48026575	1	AR01063	STOP codon acquisition
p.K301fs*12	chr2:48026024	1	AR01069	STOP codon acquisition
p.G409E	chr2:48026348	2	AR02040; AR01063	
p.P591S	chr2:48026893	1	AR02005	
p.P107L	chr2:48018125	1	AR02005	
p.P711L	chr2:48027254	1	AR02005	
p.P1097S	chr2:48030675	1	AR02005	
p.V474M	chr2:48026542	1	AR01013	
p.P1097L	chr2:48030676	1	AR01015	
p.G1292E	chr2:48033664	1	AR01015	
p.R772Q	chr2:48027437	1	AR01015	
p.G1138R	chr2:48030798	1	AR01034	
p.S405F	chr2:48026336	1	AR02040	
p.P656L	chr2:48027089	1	AR02011	
p.P656S	chr2:48027088	1	AR02064	
p.P399L	chr2:48026318	1	AR02064	
p.P838S	chr2:48027634	1	AR01063	
p.T518I	chr2:48026675	1	AR01063	
p.G477S	chr2:48026551	1	AR01063	
p.G1218D	chr2:48033349	1	AR01063	
p.G1316R	chr2:48033735	1	AR01063	
p.T407I	chr2:48026342	1	AR02007	
p.G1224E	chr2:48033367	1	AR02007	
p.T605I	chr2:48026936	1	AR02007	

American Association for Cancer Research

TMZ Signature and TMB Change as a Function of Heterogeneity in Colorectal Cancer Treated with TMZ

Metastases are highly heterogeneous, and the impact of heterogeneity on the pharmacodynamic response to TMZ priming in patients with colorectal cancer is unknown. To infer how a subset of TMZ-resistant colorectal cancer cells affected the TMB value and mutational signature 11 of the overall population, we exploited two TMZ-sensitive (TMZ-S) colorectal cancer cell lines (SKCO1 and SW620) and their TMZ-resistant (TMZ-R) derivatives that were generated by long-term drug exposure. We performed a new high-depth WES of DNA pools of both TMZ-S and TMZ-R cells composed of different fractions including 100% TMZ-R; 50% TMZ-S, 50% TMZ-R; 75% TMZ-S, 25% TMZ-R; 87.5% TMZ-S, 12.5% TMZ-R; 93.75% TMZ-S, 6.25% TMZ-R; and 100% TMZ-S. In parallel, the same populations were created *in silico* (see Methods for detail) using different ratios of sequencing reads from WES data for both TMZ-S and TMZ-R cells. The correlation between TMB obtained by cell-based and *in silico* mixture analyses was 0.9968 (Pearson product–moment correlation with $P = 2.34e-12$; Supplementary Fig. S5A), confirming the robustness of this approach.

We then studied the effect of population heterogeneity on TMB increase and TMZ signature detection in the SKCO1 TMZ-S cell line and its TMZ-R derivative. The analysis revealed that at least 30% TMZ-R cells were required to reach the TMB cutoff of 20 mut/Mb using the clonal analysis, whereas as few as 2% TMZ-R cells were sufficient using the subclonal analysis (Supplementary Fig. S5B). To be able to detect the TMZ signature, more than 25% of mutational signature 11–positive cells were required using the clonal analysis, whereas 6.25% cells were necessary to reach the subclonal threshold (Supplementary Fig. S5C and S5D). In conclusion, based on these results, when a clonal effect was detected, we expected that a 25% to 30% fraction of tumor cells to display the TMZ scar, whereas in the case of subclonal effect, we expected a fraction between 2% to 6% and 25% to 30% to display the TMZ scar.

Finally, we analyzed the impact of heterogeneity in the cell populations that acquired TMZ resistance through the copresence of two different mechanisms: the reexpression of MGMT and the acquisition of MMR gene mutations with an increase of TMB and switching from MMRp to MMRd phenotype in the SW620 cell line. In this case, when only clonal mutations were considered, there was a modest increase of TMB that did not reach the 20 mut/Mb cutoff (orange line in Supplementary Fig. S5E). When considering subclonal mutations, more than 50% TMZ-R cells were required to overcome the 20 mut/Mb cutoff (Supplementary Fig. S5E). Due to the low number of acquired mutations, TMZ mutational signature 11 could not be retrieved when we applied a VAF ≥10% threshold (clonal mutations). For the same reasons, more than 25% TMZ-R cells were required to detect the TMZ signature using subclonal alterations (Supplementary Fig. S5F). Collectively, we showed how the mutational signature 11 and TMB change as a function of the heterogeneity of the population.

The previous preclinical results showed that intratumor heterogeneity (ITH) plays a relevant role in the tissue analysis (TMB and genetic signatures), so we proposed that the differences between tissue tumor subtype B2 and B1 after TMZ treatment rely mainly on the fractional abundance of cells showing the TMZ genetic impact (Fig. 6A). Next, we addressed the impact of ITH by analyzing three different regions (corings) from the same liver lesion biopsy collected from patient AR02005 at the progression of TMZ treatment (Fig. 6B). Interestingly, the three regions belonging to the same metastasis showed different TMB values: coring A and C had lower clonal TMB of 8 mut/Mb, whereas coring B displayed 16 mut/Mb (Fig. 6C). At the subclonal level, the three TMB values were different, thus suggesting that heterogeneity has a relevant role in the TMB evaluation by tissue biopsy analysis (Fig. 6C). Of note, genetic signature analysis confirmed that the molecular effect of TMZ was clonal for coring B (Fig. 6D) with higher TMB, whereas the effect was evident only at the subclonal level for regions A and C (Fig. 6D). Venn diagrams of all genetic alterations demonstrate that corings A and C were identical at the clonal level, and these were a subset of coring B (Fig. 6E, left). On the other hand, at the subclonal level, all three regions displayed elevated heterogeneity, maintaining a core of 202 common mutations (Fig. 6E, right).

Clinical and Molecular Monitoring of Patients Treated with Pembrolizumab after TMZ Priming

The planned accrual of 20 patients to be treated with immunotherapy was disrupted by the COVID-19 pandemic. As the trial proved lengthy, we present here the first six patients treated with the anti–PD-1 pembrolizumab. Although there were no objective partial or complete responses according to the iRECIST definition (70), four patients had sustained SD as the best response, with the responses lasting for >2 years, 6.5 months, and 5.5 months for AR02007, AR01015, and AR03047, respectively, whereas AR01034 died of myocardial infarction while still progression free at 2.9 months (Fig. 7A). We thus observed a disease control in four of six heavily pretreated cases, corresponding to a DCR of 67%. To exclude that DCR could be ascribed to differences in growth kinetics of individual tumors, independent of TMZ, we calculated the growth modulation index (GMI) of the overall treatment strategy in each patient, allowing intrapatient comparison of previous time-to-progression intervals (TTP; refs. 71, 72). Interestingly, the median GMI was 1.8 (range, 1.2–7.0), and all patients treated with TMZ and pembrolizumab achieved a GMI >1.33 (cutoff of clinical meaningfulness; ref. 73) with the exception of patient AR01034, who died of other causes without signs of progression (Fig. 7B).

To longitudinally monitor the effect of pembrolizumab on TMZ-primed patients, we performed the serial molecular profiling of plasma collected at multiple time points during anti–PD-1 treatment (Fig. 7C; Supplementary Fig. S6A). In AR02007, who had long-lasting SD, we found that bTMB (at both clonal and subclonal levels) increased during TMZ-based priming treatment, declining after pembrolizumab treatment (cycle 10: clonal bTMB from 57 to 17 mut/Mb; subclonal bTMB from 2,276 to 50 mut/Mb) with a stabilization of the clonal bTMB (at cycles 10, 20, and 34, bTMB clonal was always 17 mut/Mb) and with subclonal bTMB returning approximately at baseline (prepriming) levels in the last analyzed time point
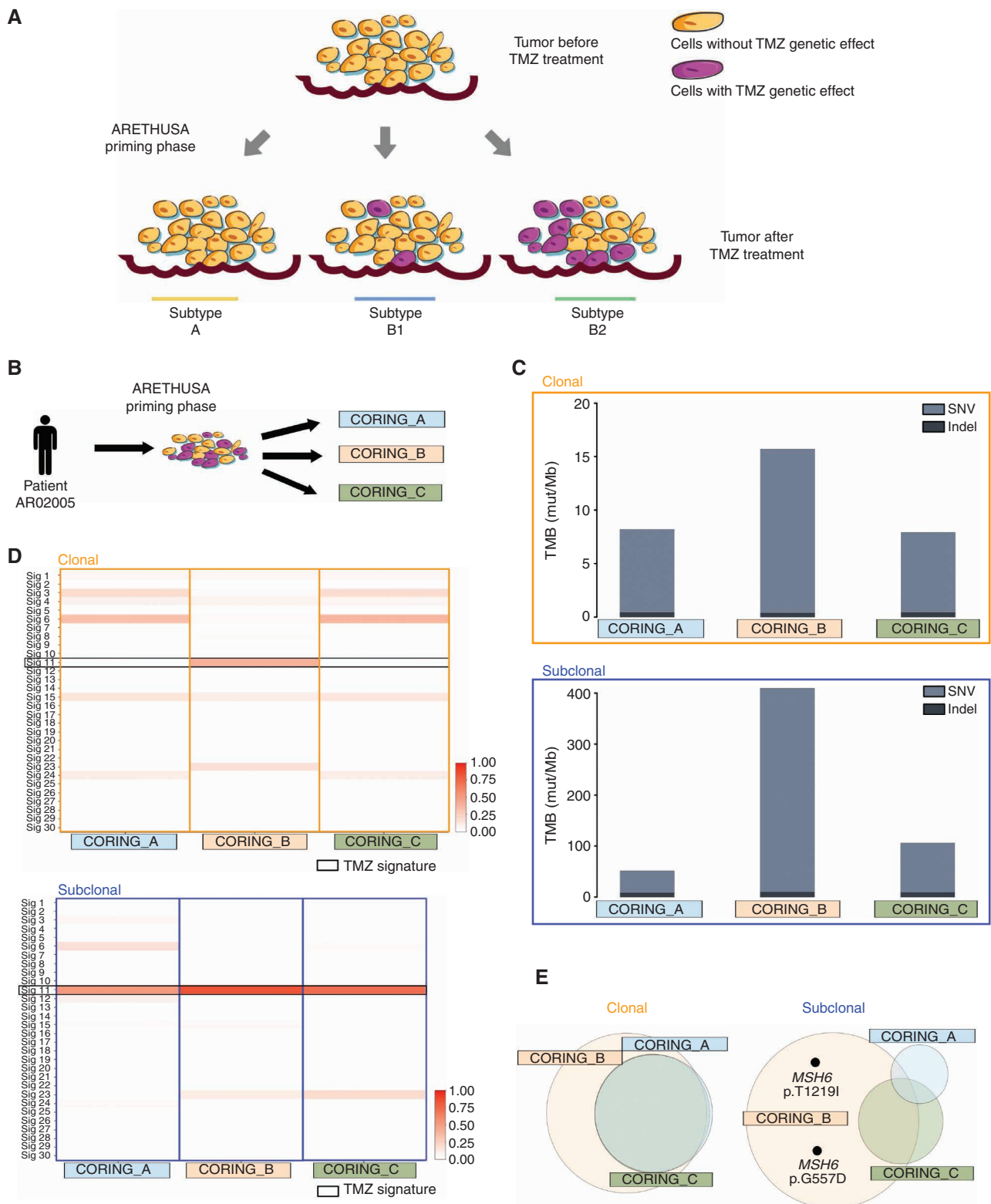
Figure 6. Molecular intralesion heterogeneity was induced by TMZ, affecting distinct regions of the same lesion in a different manner. **A,** Scheme of the proposed tumor response to TMZ treatment; the percentage of cells showing TMZ genetic effect was different in three different tumor subtypes. **B,** Scheme of the experiment. **C,** TMB in the three corings with the relative contribution of SNV/indel was reported at clonal (top) and subclonal (bottom) levels. **D,** Signature analysis at clonal (top) and subclonal (bottom) levels of the three corings. **E,** Venn diagram of common, shared, and private genetic alterations in the three corings at the clonal (left) and subclonal (right) levels. Variants *MSH6* p.T1219I and p.G557D were shown in the private mutations of subclonal coring B. Sig, signature.

American Association for Cancer Research
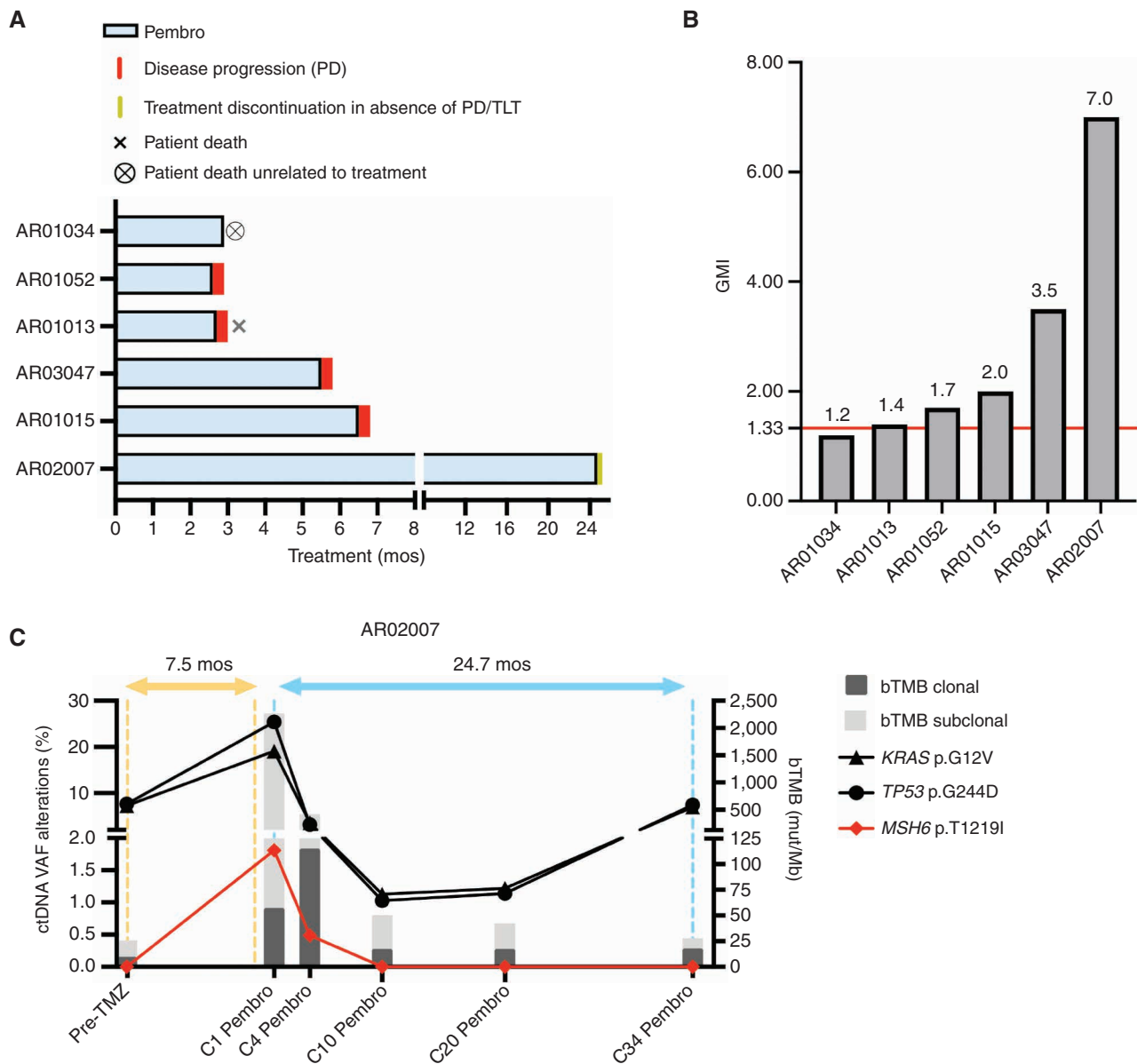
Figure 7. Clinical impact of pembrolizumab on MMRp mCRC patients after TMZ priming. **A,** Swimmer plot of six patients who achieved high TMB after TMZ priming and were treated with pembrolizumab monotherapy until progression; two patients had PD after 3 and 4 cycles, whereas three patients were treated for 7, 9, and 33 cycles with long-lasting disease stabilization before progression. One patient died from an unrelated cause, with tumor stabilization after 5 cycles. **B,** GMI for each patient primed with TMZ and treated with pembrolizumab. Red bar indicates the cutoff of 1.33, considered clinically meaningful. **C,** Graph shows the longitudinal, liquid biopsy–based ctDNA monitoring of the patient AR02007 during the priming (TMZ-based therapy) and immunotherapy (pembrolizumab) phases of ARETHUSA. Colored lines indicate the clonal evolution of trunk/driver mutations (*KRAS* and *TP53*; black) and the *MSH6* p.T1219I variant (red) detected by ctDNA analysis at the indicated time points. bTMB (clonal and subclonal) at each time point is also reported (dark and light gray bars). mos, months of treatment; Pembro, pembrolizumab; TLT, treatment-limiting toxicity.

(subclonal bTMB from 26 mut/Mb before the TMZ priming to 27 mut/Mb after pembrolizumab discontinuation; Fig. 7C). Of note, bTMB high to low switch (at both clonal and subclonal levels) is also accompanied by the emergence and decline of the *MSH6* p.T1219I variant and other MMR gene mutations, suggesting that the efficacy of ICB treatment was predominantly directed against the MMRd fraction of the tumor. Longitudinal plasma analysis of AR02007 also showed that *MSH6* p.T1219I emerged in blood upon TMZ treatment, declined

during immunotherapy treatment, and eventually disappeared after 9 pembrolizumab cycles (Fig. 7C). Conversely, in other patients achieving shorter SD as best response to pembrolizumab (AR01015 and AR03047) or experiencing PD (AR01013 and AR01052), no VAF decrease of trunk/driver mutations was observed. Longitudinal ctDNA analysis in these patients highlighted that clonal bTMB was stable during pembrolizumab treatment (AR03047: from 6 to 7 mut/Mb; AR01015: from 14 to 14 mut/Mb; AR01013: from 4 to 5 mut/Mb; AR01052 from 6

to 7 mut/Mb; Supplementary Fig. S6A), whereas longitudinal subclonal bTMB increased along with anti–PD-1 treatment in four of six cases (AR03047, AR01015, AR01013, and AR01052).

In this subset of cases, carcinoembryonic antigen (CEA) levels were monitored at multiple longitudinal time points (baseline, best response, and progression/treatment discontinuation) during both priming and immunotherapy phases. In the two patients achieving durable SD, the CEA levels accordingly decreased (AR02007) or remained unchanged compared with baseline (AR01015), whereas in two patients displaying short-lived SD, CEA either increased (AR03047) or was not altered at baseline and remained unaltered until progression (AR01034). In the two remaining patients who had PD as the best response, CEA levels rapidly increased as expected (Supplementary Fig. S6B). In AR01034, CEA levels were not indicative, as they were within the range of physiologic values (cutoff: 5 ng/mL). In the other patients, the trend of CEA levels paralleled the trend of tumor load during treatment (as assessed by radiologic evaluation by RECIST 1.1 criteria). As expected, a specific increase in CEA levels was observed concurrently with PD. A specific response in CEA levels during pembrolizumab treatment was observed only in AR02007, in whom long SD was accompanied by shrinkage of the metastatic lesions (Supplementary Fig. S6B).

DISCUSSION

In most solid tumors, TMB levels have been shown to correlate with response to ICB (74). Indeed, the FDA has approved a cancer type–agnostic use of the anti–PD-1 pembrolizumab in patients with TMB ≥10 mut/Mb (50, 74). Unfortunately, the vast majority of mCRC patients are MMRp, display a low TMB, and do not respond to anti–PD(L)-1 therapies. The ARETHUSA trial was designed to test the concept that the pharmacologic inactivation of MMR pathways could be clinically actionable. Accordingly, ARETHUSA is a proof-of-concept phase II trial testing whether a dynamic TMB increase in MSS mCRC can be obtained by therapeutic priming with the alkylating agent TMZ, potentially favoring response to ICB. This unconventional approach is based on our prior preclinical evidence showing that TMZ is active against mCRC (45, 46) and also targets the DNA repair processes resulting in both TMB and neoantigen increase in tumor cells (44). ARETHUSA was designed as a two-step study taking advantage of our previous knowledge that optimal selection for the efficacy of TMZ in mCRC is achieved by a two-layer molecular assessment of MGMT inactivation involving IHC and methylation assays (49). In the first phase of the trial, TMZ is used for both its direct antitumor effect and as a "pharmacologic primer" by inactivating MMR genes, thus leading to increased mutational burdens such as SNVs and indels. These could, in turn, lead to the generation of neoepitopes, thus sparking immune surveillance and boosting response to ICB.

In the initial analysis reported here, we studied how TMZ treatment affects the genome of MGMT-negative, *RAS*-mutated mCRC.

First, we found that the specific TMZ signature 11 emerges in post–TMZ treatment samples of mCRC patients and the effect is dependent upon the number of cycles, suggesting

that a minimum exposure level/time is required for detection of the TMZ genomic scar.

Second, we report that only patients whose tumors carried the characteristic TMZ signature developed high subclonal or clonal TMB levels. However, post-TMZ TMB measured in tissue from a single metastatic site might fail to fully capture the heterogeneity of intermetastasis and even intrametastasis response to TMZ. Indeed, our results suggest that the molecular effect of TMZ differentially affects distinct regions of the same lesion. Therefore, to capture the mutational impact of TMZ more comprehensively, we measured TMB in ctDNA and found it largely comparable with the subclonal TMB calculated by WES data obtained by a tissue biopsy. On the other hand, bTMB was influenced by ctDNA levels (see Supplementary Table S2 and Supplementary Fig. S4B). This finding tallies with the evidence that different tumors and/or metastatic sites may have a different ctDNA release capacity, thus potentially affecting bTMB analysis. Indeed, it was recently reported that both pulmonary and peritoneal metastases from colorectal cancer have significantly lower maximum allele frequencies and a lower number of cancer-specific variants in blood as compared with patients with a lesion in other metastatic sites, like the liver (64). Singularly, neither TMB (from tissue) nor bTMB (from blood) analysis is sufficient alone to correctly stratify patients. Collectively, these results suggest that an integrated analysis coupling both plasma and tissue TMB evaluation is more informative. Longitudinal CEA levels may correlate with disease burden in some patients, but they do not capture the clonal dynamics triggered by TMZ treatment.

Third, we revealed that the TMZ mutational signature is heralded by the presence in plasma and tissue of the p.T1219I variant of the MMR gene *MSH6*. Additional mutations in *MSH6* were also found exclusively in both tissue and plasma after TMZ treatment, further strengthening this association. In addition, we have highlighted the *MSH6* p.T1219I variant as a potential marker for TMZ molecular efficacy in colorectal cancer. Confirmation of this variant as a predictive marker of response should be assessed in further validation studies. In support of the "predictive" relevance of this variant, we did not observe the p.T1219I variant in patients in whom mutational signature 11 was absent after TMZ treatment, although it emerged in 94% of patients who benefited from TMZ treatment (16/17 = 94%). Further analyses corroborated this notion by revealing additional mutations in *MSH6* detected only in both tissue and ctDNA post-TMZ samples. Notably, all *MSH6* SNVs (100%) are related to the nucleotide contexts favored by signature 11.

Tantalizingly, one of the patients (AR02007) who reached a major TMB increase upon TMZ priming and then was treated with pembrolizumab achieved disease control lasting for over 2 years. The AR02007 disease stabilization was tracked in blood by following specific trunk/driver mutations (*TP53* and *KRAS*) in longitudinal plasma samples collected during treatments. This analysis highlighted the onset of the *MSH6* p.T1219I variant after TMZ-based treatment and its decline, until disappearing, during ICB treatment. Of interest, in this patient, the trend of the *MSH6* variant mirrors that of bTMB (at both clonal and subclonal levels).

Although it is conceivable that pharmacologic inactivation of the MMR pathway by TMZ is related to increased

mutational and neoantigen burdens and therefore to immune modulation, other mechanisms linking DNA damage and immune surveillance also exist (75). These include but are not limited to activation of the cGAS/STING pathway by cytosolic DNA, as recently reported for MMRd tumors (76). It is, therefore, plausible that inactivation of MMR upon pharmacologic treatment with alkylating agents such as TMZ could also trigger intracellular signaling pathways leading to innate antitumor immunity.

A major limitation of our current analysis is that owing to the limited amount of tissue available through post-TMZ biopsies, the investigations were limited to WES for TMB measurements, as we were unable to perform other analyses on the same samples. In this regard, future studies may investigate whether TMZ treatment can induce upregulation of PD-L1 and increased infiltration of IFNγ⁺CD8⁺ T cells in human tumors, as previously observed in animal models (44). Another limitation of our approach is the narrow, though existing, antitumor TMZ activity. We are planning to address this aspect by combinatorial studies in which TMZ will be associated with more active therapeutic regimens.

Finally, although we recognize that no conclusions can be made at this junction on the clinical utility of TMZ as an immune chemosensitizer, the wealth of pharmacodynamic data we produced as well as the GMI results are suggestive. The surprisingly long median TTP (the expected TTP in this population of mCRC patients pretreated with 3 or more lines of therapies is ~2 months; refs. 77, 78) is due to the growth kinetics, as suggested by the GMI >1 values in all cases. Furthermore, our findings support the recent results from the MAYA trial (NCT03832621) in *MGMT*-methylated MSS mCRC patients (79). MAYA, unlike ARETHUSA, exploited a 2-month TMZ priming phase, which was followed in the absence of PD by a combinatorial approach made of TMZ with low-dose ipilimumab plus nivolumab. Consistent with the ARETHUSA patient cohort, approximately one fourth of the MAYA patients primed with TMZ eventually received immunotherapy (79). The primary endpoint of the 8-month PFS rate in the MAYA trial was met, reaching a notable 36% compared with a historical 5%, and a median PFS was 7 months, possibly favored by the use of an anti–PD-1 and anti-CTLA4 combination or to an earlier start of immunotherapy (80, 81). Interestingly enough, the analysis of tumor-paired biopsies, albeit limited to the TMB assessment and conducted in only four patients, showed an acquired high TMB (79).

In summary, we provide a proof-of-concept that the inactivation of genes involved in DNA repair can be achieved pharmacologically with TMZ treatment, while offering potential clinical benefit to patients with *MGMT*-methylated, *RAS*-mutant mCRC refractory to SOC treatments. We also show that the priming process can be monitored in tissue and blood samples, providing initial evidence of a blood biomarker used to effectively measure the effectiveness of MMR inactivation. Although the ARETHUSA trial is not completed yet, the multidimensional translational analyses presented here show that increased mutational burdens can be achieved by pharmacologic modulation in *RAS*-mutant, MSS colorectal cancers with an initial low baseline TMB. Additional studies are needed to confirm the relevance and applicability of this approach for the treatment of *RAS*-mutant, MSS mCRC.

METHODS

The ARETHUSA Trial

Institutional review boards of all participating institutions (Niguarda Cancer Center, Grande Ospedale Metropolitano Niguarda, Milan; Fondazione IRCCS Istituto Nazionale dei Tumori, Milan; HUMANITAS Research Hospital, Rozzano and IEO Istituto Europeo di Oncologia, Milano) approved the study procedure. All patients provided written informed consent for participation in the study and associated procedures. The study was conducted in accordance with the principles of the Declaration of Helsinki and the International Conference on Harmonisation and Good Clinical Practice guidelines. The ARETHUSA trial (NCT03519412; EudraCT number 2018-001441-14) is sponsored by IFOM, the FIRC Institute of Molecular Oncology, and was approved by the local ethical committee and the Italian Competent Authority (AIFA) on October 29, 2018.

In the screening phase of ARETHUSA (NCT03519412), patients with *RAS*-extended (*KRAS* or *NRAS*, exons 2, 3, 4) mutant MSS/MMRp mCRC were tested for MGMT status in tissue by IHC (49) and methyl-BEAMing (see the following section). Patients with MGMT IHC staining negative and methylated *MGMT* promoter were enrolled in the priming phase and underwent treatment with oral TMZ (150 mg/m²/day; days 1–5 every 28 days; Fig. 1) until disease progression or unacceptable toxicity. Disease progression was determined according to RECIST 1.1 (82).

At disease progression or treatment discontinuation, a mandatory biopsy was performed to evaluate TMB. Only MSS/MMRp patients with tumor mutational load ≥20 mutations/Mb after TMZ treatment were enrolled in the immunotherapy phase and received intravenous anti–PD-1 blockade by pembrolizumab monotherapy (200 mg every 3 weeks) until disease progression, until unacceptable toxicity, or up to 24 months in patients without disease progression (Fig. 1).

Of note, two liquid biopsies for the experimental NGS-based determination of the molecular profiling and bTMB were collected before and after treatment (Fig. 1).

Methyl-BEAMing Assay

Five hundred nanograms of DNA were used for bisulfite conversion using the EZ DNA Methylation-Gold Kit (Zymo Research) following the manufacturer's protocol, with final elution in 70 μL. Bisulfite-converted DNA was assessed via methyl-BEAMing for the methylation status of the *MGMT* gene. Methyl-BEAMing analysis is a multistep digital PCR–based technique (83). A first amplification allows the enrichment of the locus of interest and is carried out using tagged primers. Amplicons are then diluted (1/16,000) and resubjected to PCR amplification using the tag and tag-coated beads. The second round of amplification is performed in emulsion, allowing the physical separation and independent amplification of the different templates. PCR mixes are prepared according to the conditions described (84). Next, the emulsion is broken using alcohol-based buffers (isopropanol/butanol), and amplicons are hybridized with fluorescent probes specific for the methylated or unmethylated bisulfite-converted templates. Fluorescence is then assessed on an Accuri C6 flow cytometer (BD) using the filters previously established with controls (scale of methylation). The percentage of methylation is calculated by dividing the number of methylated specific events by the sum of methylated plus unmethylated specific events. A minimum of 200 cumulative events (methylated + unmethylated) are required for a result to be considered valid. Quantification ability and linearity of the methyl-BEAMing assay were previously tested with a scale made of the template corresponding to the fully methylated or unmethylated bisulfite-converted sequence (84). The threshold for calling a sample positive was set at 34.5% based on the expected clinical benefit observed in MGMT IHC-negative patients that has been reported (49).

Cell Lines and In Vitro Drug Treatments

SKCO1 and SW620 colorectal cancer cell lines are part of a large collection that we previously described (85). Cells were routinely supplemented with FBS 10% 2 mmol/L L-glutamine and antibiotics (100 U/mL penicillin and 100 mg/mL streptomycin) and grown in a 37°C and 5% CO_2 air incubator. Cells were routinely screened for the absence of *Mycoplasma* contamination using the Venor GeM Classic kit (Minerva Biolabs). The identity of each cell line was checked using the PowerPlex 16 HS System (Promega), through short tandem repeat (STR) tests at 16 different loci (D5S818, D13S317, D7S820, D16S539, D21S11, vWA, TH01, TPOX, CSF1PO, D18S51, D3S1358, D8S1179, FGA, Penta D, Penta E, and amelogenin). Amplicons from multiplex PCRs were separated by capillary electrophoresis (3730 DNA Analyzer, Applied Biosystems) and analyzed using GeneMapper v.3.7 software (Life Technologies).

Cells were cultured with 100 μmol/L of TMZ until they acquired resistance as previously described (44). When resistance seemed acquired, a scalar concentration of the drug was assessed to verify the increase in IC_{50} compared with parental TMZ. At this point, the identity of the cell line was checked through STR profiling (Promega). Then, in order to evaluate the mutational signature acquired after treatment refractoriness, two million resistant cells were seeded in a 10-cm dish in media without the drug for 21 days and then were collected, and DNA was extracted for WES.

NGS Workflow and WES Data Generation

QIAamp DNA Blood Mini Kit (Qiagen) was used for DNA extraction from PBMC and fresh tissue. The preparation was performed following the manufacturer's protocol. Starting from 200 ng of DNA from fresh tissue/PBMCs, NGS libraries were prepared using the Nextera DNA Flex Library Prep Kit (Illumina) according to the manufacturer's protocol. Subsequent whole exome target enrichment was performed following IDT xGen protocol (xGen Hybridization and Wash Kit, xGen Universal Blockers-NXT Mix, xGen Exome Research Panel v2; IDT, Inc.). The quality of libraries was checked with the High-Sensitivity DNA assay kit (Agilent Technologies). Library preparation, enrichment of whole exome regions, and sequencing of patient samples were performed by Cogentech Società Benefit srl.

NGS libraries for cell line samples were prepared starting with 150 ng of DNA and processed with Illumina DNA Prep with Enrichment and Exome Panel 45 Mb (Illumina) according to the manufacturer's protocol. After the fragmentation of gDNA with transposon enzyme and subsequent PCR to introduce unique sample indexes, DNA fragment size distribution was assessed using the 2100 Bioanalyzer with a High-Sensitivity DNA assay kit (Agilent Technologies). Equal amounts of DNA libraries were pooled and subjected to targeted panel hybridization capture.

Final libraries were sequenced on NextSeq sequencer 500 or 550 DX (Illumina).

Genetic Analysis of Tissue: Mutational Profiling and TMB Analysis

"Fastq files" were generated using the bcl2fastq command, and the high-depth sequencing data were obtained (Supplementary Table S1). Fastq files were processed using the genomic analysis workflow for precision oncology as previously described (67, 68). The BWA-mem algorithm was used to map reads to the human genome version 19 (hg19), and PCR duplicates were removed using the RMDUP command in the SAMtools bioinformatic suite. To delete NGS artifacts (86), reads having more than 3 different mismatches and bases with quality PhredScore <30 were not considered in the mutations calling step. Mutations supported only by alteration falling in the first/last reads position were filtered, and strand bias correction was applied as previously described (68). The Pindel tool was used for the indels calling. After the filtering step (where

NGS artifacts were filtered out), a median depth 376× and coverage ≥96.82% at 100× depth with a median of 124 million reads per sample were obtained (Supplementary Table S1).

Alignments from PBMCs and tissue tumor samples were compared to identify mutations/indels in tumor and matched normal samples. Germline mutations were common to both samples, whereas somatic alterations were present only in the tumor. For cell line analysis, mutation calling was performed using hg19 as a reference and filtering out all mutations reported in the dbSNP (v147). In the section "TMZ Signature and TMB Change as a Function of Heterogeneity in Colorectal Cancer Treated with TMZ," in order to consider only the acquired mutations, two independent sequencing experiments of the same parental cell line were performed in order to use one parental cell line as reference.

All the VAFs reported in the text were adjusted using the copy-number variation data (tumor vs. germinal). In order to verify the diploidy of the germinal DNA of each patient, the ploidy analysis was performed. Large copy-number alterations were identified by the aneuploidy score, defined as the sum of the number of altered chromosome arms (87). All chromosomes of 21 germinal PBMCs obtained the lowest values (score 0, all arms of autosomal chromosomes were diploid). Focal ploidy was identified based on the copy-number analysis of germline DNA from PBMCs in comparison with a metanormal built from 21 PBMCs sequenced using the same "wet" procedures. This comparison was used for the correction of different probes' affinity.

Finally, tumor focal gene copy-number variations analysis was performed in the matched samples (tumor vs. germinal) for each patient. Gene copy number was calculated as the ratio of median gene depth and the median depth of all genes in the whole exome. For each gene, the copy-number alteration was calculated as the ratio between the copy number of normal tissue and copy number of the same gene in the tumor samples as previously reported (67, 68). Tumor copy number was considered altered when the log_2 value was higher than 1 or lower than −1. On the basis of the copy-number variation, VAF of all the mutations falling into altered regions were then normalized. Overall, as expected, no gene amplifications or deep deletions were reported in the tumor tissue biopsy collected after TMZ treatment. In detail, only slight and focal copy-number increases/decreases were reported in the tumor patient cohort, with a median value of 0.00696011% (or mean of 0.1820%) of altered genomic regions.

TMB was calculated from WES data taking into consideration nucleotide variants with a 5% significance level obtained with a Fisher test and supported by a minimum of four mutated reads in regions with a minimum depth of 5×. We considered only mutations with an adjusted allele frequency ≥10% for clonal analysis and ≥1% for subclonal analysis, excluding mutations annotated in dbSNP (v147). All data were normalized on the real target regions as previously described (6, 44, 68, 88).

We performed another type of normalization using a sliding cutoff (not the 10% fixed cutoff) in order to check if another method of cell purity calculation could influence our clonal/subclonal results. In detail, we normalized TMB on the basis of the purity calculation as described in ref. 89. The clonal/subclonal TMB and mutational signature results were also confirmed using this alternative approach based on ref. 89, with respect to this article's method (Supplementary Fig. S7A and S7B). In conclusion, using an alternative method, the tumor patients' stratification in A, B1, and B2 subtypes based on clonal/subclonal results was confirmed.

Mutational Signature Analysis

Only alterations with fractional abundance ≥10% were used for clonal analysis, whereas alterations with fractional abundance ≥1% were used for subclonal analysis. The matrix with mutation contexts was built using sigprofilerMatrixGenerator (90).

Using the information of somatic SNVs in the matrix, a series of mutational profiles was extracted, and genetic signatures were

calculated using the MuSiCa tool (91) and Mutational Patterns package (59). COSMIC signature references v. 2.0, v 3.0, and v. 3.2 were used for the fitting in the mutational signature analysis. For clonal analysis in five cases (AR02071, AR01032, AR01014, AR01069, and AR02064), the number of mutations was not sufficient to perform the supported mutational analysis (cosine similarity lower than 0.9), and these five samples were excluded. The clonal mutations (with VAF ≥10%) were not enough to perform signature analysis in some samples of the SW620/SKCO1 cell lines.

Cosine similarity between two vectors of the same length was calculated using the MuSiCa (91) and Mutational Patterns tools (59). The cosine was used to evaluate the similarity between the original mutational profile (obtained by the mutations identified in the sample) and the reconstructed mutational profile based on the optimal linear combination of all COSMIC signatures identified after fitting (59, 60). All mutations with allelic frequencies ≥1% (for subclonal analysis) and ≥10% (for clonal analysis) were also used to build a distance matrix that was the starting point to build the agglomerative hierarchical clustering. The "Cluster" package of the R software (freely available at www.r-project.org) and the unweighted pair group average method (UPGMA) were used.

For the enrichment analysis of the signature 11 contexts in the APC and MMR genes, we started dividing the nucleotide sequence of each gene (sliding window) in the three nucleotide (triplet) contexts that then were extracted to consider the fractional abundance of each context in the genes. Contexts ACC; ACT; AGA; AGG; AGT; CAA; CCC; CCG; CCT; CGG; GCA; GCC; GGA; GGC; GGG; GGT; TCA; TCC; TGA; TGC; TGG were considered "favored by signature 11" on the base of the mutation probability reported for signature 11 (57).

TMB/Signature Detection in Preclinical Models

To simulate a mixed population of colorectal cancer cell models (sensitive and resistant to TMZ) "in silico" NGS databases were established. FastQ files for each population were created using different percentages of sequencing reads obtained by 100% TMZ-S parental and 100% TMZ-R cells from sequencing data by SW620 and SKCO1 cell lines. The six populations were composed as follows: 100% TMZ-R (1), 50% TMZ-R + 50% TMZ-S (2), 25% TMZ-R + 75% TMZ-S (3), 12.5% TMZ-R + 87.5% TMZ-S (4), 6.25% TMZ-R and 93.75% TMZ-S (5), and 100% TMZ-S (6). A fixed number of 100,663,296 reads was always used as the total number of reads, whereas the ratio of reads was derived from resistant/sensitive cells. With this method, we created the paired fastQ files for each mixed population. Starting from in silico fastQ files, each population was then analyzed as previously reported.

ctDNA Mutational Profiling and bTMB Analysis

Whole blood samples were collected in K2-EDTA tubes before patients started TMZ treatment (baseline, pre-TMZ) and/or at the time of disease progression (post-TMZ). Plasma was isolated from the cellular component and frozen. Frozen plasma samples were shipped to Guardant Health for cell-free DNA extraction and mutational profiling. Extracted cfDNA was analyzed using the GuardantOMNI research-use-only (RUO) NGS assay (Guardant Health) to identify SNVs, indels, gene fusions, copy-number variants, microsatellite status, and bTMB across a 2.145 Mb panel. bTMB was reported as variations per megabase (mut/Mb) by the GuardantOMNI algorithm (63), which includes all somatic synonymous and nonsynonymous SNVs and indels, filtering out and excluding germline, clonal hematopoiesis of indeterminate potential, and known driver and resistance variations. Statistical adjustment for and sample-specific tumor shedding and molecular coverage, as well as normalization by panel size, was performed (63). Further details are available in ref. 63.

bTMB was further divided into the clonal (using the sliding cutoff of 10% of the tumor content identified in the sample) and subclonal counterparts.

GMI Calculation

The GMI was defined as previously described (92). Briefly, a comparison of PFS on overall ARETHUSA strategy treatment (TMZ and pembrolizumab; PFS_n) versus PFS on prior therapy (PFS_{n-1}) was performed. A GMI >1.33, that is, an increase in the PFS_n/PFS_{n-1} ratio of 30%, was considered clinically meaningful (72).

Statistical Analysis

Statistical analysis was performed using R (version 3.6.3 and 4.0.3). The individual statistical tests used are specified in the relevant Results section and figure legends.

Spearman rank correlation was performed between the number of mutations/megabase induced by TMZ signature (normalized_score_SBS11 * TMB from only SNVs) and TMZ courses in patients (Fig. 3C; $P = 2.535e-5$ and $R = 0.7847$) and in the methodologies' comparison in Supplementary Fig. S7B ($R = 0.9653$ and $P = 2.2e-16$). The Wilcoxon rank-sum test was used to compare bTMB in matched pre–post TMZ plasma samples ($P = 0.002443$; Fig. 4D and E). Pearson product–moment correlation ($P = 2.34e-12$; Supplementary Fig. S5A) was used for the correlation between TMB obtained by cell-based and in silico analyses.

Data and Software Availability

Bioinformatic codes are available at https://bitbucket.org/irccit/idea/src/master/.

Human sequencing data are available at the European Genome-phenome Archive (EGA) under study ID EGAS00001002694 (https://www.ebi.ac.uk/ega/home) and the European Nucleotide Archive under accession numbers PRJEB33045 and PRJEB46380 (https://www.ebi.ac.uk/ena/browser/search).

Authors' Disclosures

Authors' Contributions

G. Crisafulli: Conceptualization, resources, data curation, software, formal analysis, investigation, visualization, methodology, writing–original draft, writing–review and editing. **A. Sartore-Bianchi:** Resources. **L. Lazzari:** Resources, data curation, visualization, project administration, writing–review and editing. **F. Pietrantonio:** Resources. **A. Amatu:** Resources. **M. Macagno:** Investigation. **L. Barault:** Investigation. **A. Cassingena:** Resources. **A. Bartolini:** Investigation. **P. Luraghi:** Project administration. **G. Mauri:** Writing–original draft, writing–review and editing. **P. Battuello:** Investigation. **N. Personeni:** Resources. **M.G. Zampino:** Resources. **V. Pessei:** Investigation. **P.P. Vitiello:** Writing–review and editing. **F. Tosi:** Resources. **L. Idotta:** Resources. **F. Morano:** Resources. **E. Valtorta:** Investigation. **E. Bonoldi:** Investigation. **G. Germano:** Conceptualization, writing–review and editing. **F. Di Nicolantonio:** Conceptualization, supervision, funding acquisition, writing–review and editing. **S. Marsoni:** Conceptualization, data curation, supervision, writing–original draft, writing–review and editing. **S. Siena:** Conceptualization, resources, supervision, writing–review and editing. **A. Bardelli:** Conceptualization, data curation, supervision, funding acquisition, visualization, writing–original draft, writing–review and editing.

Acknowledgments

REFERENCES

1. Siegel RL, Miller KD, Fuchs HE, Jemal A. Cancer statistics, 2021. CA Cancer J Clin 2021;71:7–33.
2. Sung H, Ferlay J, Siegel RL, Laversanne M, Soerjomataram I, Jemal A, et al. Global cancer statistics 2020: GLOBOCAN estimates of incidence and mortality worldwide for 36 cancers in 185 countries. CA Cancer J Clin 2021;71:209–49.
3. Yoshino T, Arnold D, Taniguchi H, Pentheroudakis G, Yamazaki K, Xu RH, et al. Pan-Asian adapted ESMO consensus guidelines for the management of patients with metastatic colorectal cancer: a JSMO-ESMO initiative endorsed by CSCO, KACO, MOS, SSO and TOS. Ann Oncol 2018;29:44–70.
4. Benson AB, Venook AP, Al-Hawary MM, Arain MA, Chen YJ, Ciombor KK, et al. Colon cancer, version 2.2021, NCCN clinical practice guidelines in oncology. J Natl Compr Canc Netw 2021;19:329–59.
5. Sartore-Bianchi A, Trusolino L, Martino C, Bencardino K, Lonardi S, Bergamo F, et al. Dual-targeted therapy with trastuzumab and lapatinib in treatment-refractory, KRAS codon 12/13 wild-type, HER2-positive metastatic colorectal cancer (HERACLES): a proof-of-concept, multicentre, open-label, phase 2 trial. Lancet Oncol 2016;17:738–46.
6. Siravegna G, Lazzari L, Crisafulli G, Sartore-Bianchi A, Mussolin B, Cassingena A, et al. Radiologic and genomic evolution of individual metastases during HER2 blockade in colorectal cancer. Cancer Cell 2018;34:148–62.
7. Kopetz S, Grothey A, Yaeger R, Van Cutsem E, Desai J, Yoshino T, et al. Encorafenib, binimetinib, and cetuximab in. N Engl J Med 2019; 381:1632–43.
8. Mauri G, Bonazzina E, Amatu A, Tosi F, Bencardino K, Gori V, et al. The evolutionary landscape of treatment for BRAF^{V600E} mutant metastatic colorectal cancer. Cancers 2021;13:137.
9. Siena S, Di Bartolomeo M, Raghav K, Masuishi T, Loupakis F, Kawakami H, et al. Trastuzumab deruxtecan (DS-8201) in patients with HER2-expressing metastatic colorectal cancer (DESTINY-CRC01): a multicentre, open-label, phase 2 trial. Lancet Oncol 2021; 22:779–89.
10. Ganesh K, Stadler ZK, Cercek A, Mendelsohn RB, Shia J, Segal NH, et al. Immunotherapy in colorectal cancer: rationale, challenges and potential. Nat Rev Gastroenterol Hepatol 2019;16:361–75.
11. Koopman M, Kortman GA, Mekenkamp L, Ligtenberg MJ, Hoogerbrugge N, Antonini NF, et al. Deficient mismatch repair system in patients with sporadic advanced colorectal cancer. Br J Cancer 2009;100:266–73.
12. Sinicrope FA, Sargent DJ. Molecular pathways: microsatellite instability in colorectal cancer: prognostic, predictive, and therapeutic implications. Clin Cancer Res 2012;18:1506–12.
13. Jiricny J. The multifaceted mismatch-repair system. Nat Rev Mol Cell Biol 2006;7:335–46.
14. Cohen R, Rousseau B, Vidal J, Colle R, Diaz LA, André T. Immune checkpoint inhibition in colorectal cancer: microsatellite instability and beyond. Target Oncol 2020;15:11–24.
15. Network CGA. Comprehensive molecular characterization of human colon and rectal cancer. Nature 2012;487:330–7.
16. Rospo G, Lorenzato A, Amirouchene-Angelozzi N, Magrì A, Cancelliere C, Corti G, et al. Evolving neoantigen profiles in colorectal cancers with DNA repair defects. Genome Med 2019;11:42.
17. Llosa NJ, Cruise M, Tam A, Wicks EC, Hechenbleikner EM, Taube JM, et al. The vigorous immune microenvironment of microsatellite instable colon cancer is balanced by multiple counter-inhibitory checkpoints. Cancer Discov 2015;5:43–51.
18. Gryfe R, Kim H, Hsieh ET, Aronson MD, Holowaty EJ, Bull SB, et al. Tumor microsatellite instability and clinical outcome in young patients with colorectal cancer. N Engl J Med 2000;342:69–77.
19. André T, Shiu KK, Kim TW, Jensen BV, Jensen LH, Punt C, et al. Pembrolizumab in microsatellite-instability-high advanced colorectal cancer. N Engl J Med 2020;383:2207–18.
20. Lenz HJ, Van Cutsem E, Luisa Limon M, Wong KYM, Hendlisz A, Aglietta M, et al. First-line nivolumab plus low-dose ipilimumab for microsatellite instability-high/mismatch repair-deficient metastatic colorectal cancer: the phase II CheckMate 142 study. J Clin Oncol 2022;40:161–70.
21. Le DT, Kim TW, Van Cutsem E, Geva R, Jäger D, Hara H, et al. Phase II open-label study of pembrolizumab in treatment-refractory, microsatellite instability-high/mismatch repair-deficient metastatic colorectal cancer: KEYNOTE-164. J Clin Oncol 2020;38:11–9.
22. Overman MJ, Lonardi S, Wong KYM, Lenz HJ, Gelsomino F, Aglietta M, et al. Durable clinical benefit with nivolumab plus ipilimumab in

DNA mismatch repair-deficient/microsatellite instability-high metastatic colorectal cancer. J Clin Oncol 2018;36:773–9.

23. Ghaus A, Pheely A, Murdock V, Shareef H, Samuel LM, Clive S, et al. Real-world experience of pembrolizumab in microsatellite instability-high CRC: a Scottish multicenter analysis. J Clin Oncol 2022;40:54.

24. Rousseau B, Foote MB, Maron SB, Diplas BH, Lu S, Argilés G, et al. The spectrum of benefit from checkpoint blockade in hypermutated tumors. N Engl J Med 2021;384:1168–70.

25. Le DT, Uram JN, Wang H, Bartlett BR, Kemberling H, Eyring AD, et al. PD-1 blockade in tumors with mismatch-repair deficiency. N Engl J Med 2015;372:2509–20.

26. Oki E, Makiyama A, Miyamoto Y, Kotaka M, Kawanaka H, Miwa K, et al. Trifluridine/tipiracil plus bevacizumab as a first-line treatment for elderly patients with metastatic colorectal cancer (KSCC1602): a multicenter phase II trial. Cancer Med 2021;10:454–61.

27. Bourhis J, Stein A, Paul de Boer J, Van Den Eynde M, Gold KA, Stintzing S, et al. Avelumab and cetuximab as a therapeutic combination: an overview of scientific rationale and current clinical trials in cancer. Cancer Treat Rev 2021;97:102172.

28. Cousin S, Cantarel C, Guegan JP, Gomez-Roca C, Metges JP, Adenis A, et al. Regorafenib-avelumab combination in patients with microsatellite stable colorectal cancer (REGOMUNE): a single-arm, open-label, phase II trial. Clin Cancer Res 2021;27:2139–47.

29. Chen EX, Jonker DJ, Loree JM, Kennecke HF, Berry SR, Couture F, et al. Effect of combined immune checkpoint inhibition vs best supportive care alone in patients with advanced colorectal cancer: the Canadian Cancer Trials Group CO.26 Study. JAMA Oncol 2020;6:831–8.

30. Marmorino F, Boccaccino A, Germani MM, Falcone A, Cremolini C. Immune checkpoint inhibitors in pMMR metastatic colorectal cancer: a tough challenge. Cancers 2020;12:2317.

31. Stupp R, Brada M, van den Bent MJ, Tonn JC, Pentheroudakis G, ESMO Guidelines Working Group. High-grade glioma: ESMO Clinical Practice Guidelines for diagnosis, treatment and follow-up. Ann Oncol 2014;25 Suppl 3:iii93–101.

32. Pavel M, Öberg K, Falconi M, Krenning EP, Sundin A, Perren A, et al. Gastroenteropancreatic neuroendocrine neoplasms: ESMO Clinical Practice Guidelines for diagnosis, treatment and follow-up. Ann Oncol 2020;31:844–60.

33. Swetter SM, Thompson JA, Albertini MR, Barker CA, Baumgartner J, Boland G, et al. NCCN guidelines® insights: melanoma: cutaneous, version 2.2021. J Natl Compr Canc Netw 2021;19:364–76.

34. von Mehren M, Kane JM, Bui MM, Choy E, Connelly M, Dry S, et al. NCCN guidelines insights: soft tissue sarcoma, version 1.2021. J Natl Compr Canc Netw 2020;18:1604–12.

35. Nabors LB, Portnow J, Ahluwalia M, Baehring J, Brem H, Brem S, et al. Central nervous system cancers, version 3.2020, NCCN Clinical Practice Guidelines in Oncology. J Natl Compr Canc Netw 2020;18:1537–70.

36. Casali PG, Bielack S, Abecassis N, Aro HT, Bauer S, Biagini R, et al. Bone sarcomas: ESMO-PaedCan-EURACAN Clinical Practice Guidelines for diagnosis, treatment and follow-up. Ann Oncol 2018;29:iv79–95.

37. Gronchi A, Miah AB, Dei Tos AP, Abecassis N, Bajpai J, Bauer S, et al. Soft tissue and visceral sarcomas: ESMO-EURACAN-GENTURIS Clinical Practice Guidelines for diagnosis, treatment and follow-up. Ann Oncol 2021;32:1348–65.

38. Hunter C, Smith R, Cahill DP, Stephens P, Stevens C, Teague J, et al. A hypermutation phenotype and somatic MSH6 mutations in recurrent human malignant gliomas after alkylator chemotherapy. Cancer Res 2006;66:3987–91.

39. Yip S, Miao J, Cahill DP, Iafrate AJ, Aldape K, Nutt CL, et al. MSH6 mutations arise in glioblastomas during temozolomide therapy and mediate temozolomide resistance. Clin Cancer Res 2009;15:4622–9.

40. Indraccolo S, Lombardi G, Fassan M, Pasqualini L, Giunco S, Marcato R, et al. Genetic, epigenetic, and immunologic profiling of MMR-deficient relapsed glioblastoma. Clin Cancer Res 2019;25:1828–37.

41. Cahill DP, Levine KK, Betensky RA, Codd PJ, Romany CA, Reavie LB, et al. Loss of the mismatch repair protein MSH6 in human glioblastomas is associated with tumor progression during temozolomide treatment. Clin Cancer Res 2007;13:2038–45.

42. Johnson BE, Mazor T, Hong C, Barnes M, Aihara K, McLean CY, et al. Mutational analysis reveals the origin and therapy-driven evolution of recurrent glioma. Science 2014;343:189–93.

43. Wang J, Cazzato E, Ladewig E, Frattini V, Rosenbloom DI, Zairis S, et al. Clonal evolution of glioblastoma under therapy. Nat Genet 2016;48:768–76.

44. Germano G, Lamba S, Rospo G, Barault L, Magrì A, Maione F, et al. Inactivation of DNA repair triggers neoantigen generation and impairs tumour growth. Nature 2017;552:116–20.

45. Amatu A, Barault L, Moutinho C, Cassingena A, Bencardino K, Ghezzi S, et al. Tumor MGMT promoter hypermethylation changes over time limit temozolomide efficacy in a phase II trial for metastatic colorectal cancer. Ann Oncol 2016;27:1062–7.

46. Amatu A, Sartore-Bianchi A, Moutinho C, Belotti A, Bencardino K, Chirico G, et al. Promoter CpG island hypermethylation of the DNA repair enzyme MGMT predicts clinical response to dacarbazine in a phase II study for metastatic colorectal cancer. Clin Cancer Res 2013;19:2265–72.

47. Pietrantonio F, Perrone F, de Braud F, Castano A, Maggi C, Bossi I, et al. Activity of temozolomide in patients with advanced chemorefractory colorectal cancer and MGMT promoter methylation. Ann Oncol 2014;25:404–8.

48. Pietrantonio F, Randon G, Romagnoli D, Di Donato S, Benelli M, de Braud F. Biomarker-guided implementation of the old drug temozolomide as a novel treatment option for patients with metastatic colorectal cancer. Cancer Treat Rev 2020;82:101935.

49. Sartore-Bianchi A, Pietrantonio F, Amatu A, Milione M, Cassingena A, Ghezzi S, et al. Digital PCR assessment of MGMT promoter methylation coupled with reduced protein expression optimises prediction of response to alkylating agents in metastatic colorectal cancer patients. Eur J Cancer 2017;71:43–50.

50. Marabelle A, Fakih M, Lopez J, Shah M, Shapira-Frommer R, Nakagawa K, et al. Association of tumour mutational burden with outcomes in patients with advanced solid tumours treated with pembrolizumab: prospective biomarker analysis of the multicohort, open-label, phase 2 KEYNOTE-158 study. Lancet Oncol 2020;21:1353–65.

51. Morano F, Corallo S, Niger M, Barault L, Milione M, Berenato R, et al. Temozolomide and irinotecan (TEMIRI regimen) as salvage treatment of irinotecan-sensitive advanced colorectal cancer patients bearing MGMT methylation. Ann Oncol 2018;29:1800–6.

52. Pietrantonio F, Lobefaro R, Antista M, Lonardi S, Raimondi A, Morano F, et al. Capecitabine and temozolomide versus FOLFIRI in RAS-mutated, MGMT-methylated metastatic colorectal cancer. Clin Cancer Res 2020;26:1017–24.

53. Alexandrov LB, Nik-Zainal S, Wedge DC, Aparicio SA, Behjati S, Biankin AV, et al. Signatures of mutational processes in human cancer. Nature 2013;500:415–21.

54. Alexandrov LB, Kim J, Haradhvala NJ, Huang MN, Tian Ng AW, Wu Y, et al. The repertoire of mutational signatures in human cancer. Nature 2020;578:94–101.

55. Davies H, Glodzik D, Morganella S, Yates LR, Staaf J, Zou X, et al. HRDetect is a predictor of BRCA1 and BRCA2 deficiency based on mutational signatures. Nat Med 2017;23:517–25.

56. Nik-Zainal S, Alexandrov LB, Wedge DC, Van Loo P, Greenman CD, Raine K, et al. Mutational processes molding the genomes of 21 breast cancers. Cell 2012;149:979–93.

57. Alexandrov LB, Nik-Zainal S, Wedge DC, Campbell PJ, Stratton MR. Deciphering signatures of mutational processes operative in human cancer. Cell Rep 2013;3:246–59.

58. Petljak M, Alexandrov LB, Brammeld JS, Price S, Wedge DC, Grossmann S, et al. Characterizing mutational signatures in human cancer cell lines reveals episodic APOBEC mutagenesis. Cell. 2019;176:1282–94.

59. Blokzijl F, Janssen R, van Boxtel R, Cuppen E. MutationalPatterns: comprehensive genome-wide analysis of mutational processes. Genome Med 2018;10:33.

60. Islam SMA, Alexandrov LB. Bioinformatic methods to identify mutational signatures in cancer. Methods Mol Biol 2021;2185:447–73.

61. Siravegna G, Mussolin B, Venesio T, Marsoni S, Seoane J, Dive C, et al. How liquid biopsies can change clinical practice in oncology. Ann Oncol 2019;30:1580–90.

62. Di Nicolantonio F, Vitiello PP, Marsoni S, Siena S, Tabernero J, Trusolino L, et al. Precision oncology in metastatic colorectal cancer—from biology to medicine. Nat Rev Clin Oncol 2021;18:506–25.

63. Si H, Kuziora M, Quinn KJ, Helman E, Ye J, Liu F, et al. A blood-based assay for assessment of tumor mutational burden in first-line metastatic NSCLC treatment: results from the MYSTIC study. Clin Cancer Res 2021;27:1631–40.

64. Bando H, Nakamura Y, Taniguchi H, Shiozawa M, Yasui H, Esaki T, et al. Impact of a metastatic site on circulating tumor DNA (ctDNA) analysis in patients (pts) with metastatic colorectal cancer (mCRC). J Clin Oncol 39, 2021 (suppl 15; abstr 3554).

65. Misale S, Yaeger R, Hobor S, Scala E, Janakiraman M, Liska D, et al. Emergence of KRAS mutations and acquired resistance to anti-EGFR therapy in colorectal cancer. Nature 2012;486:532–6.

66. Oddo D, Siravegna G, Gloghini A, Vernieri C, Mussolin B, Morano F, et al. Emergence of MET hyper-amplification at progression to MET and BRAF inhibition in colorectal cancer. Br J Cancer 2017;117: 347–52.

67. Corti G, Bartolini A, Crisafulli G, Novara L, Rospo G, Montone M, et al. A genomic analysis workflow for colorectal cancer precision oncology. Clin Colorectal Cancer 2019;18:91–101.e3.

68. Crisafulli G, Mussolin B, Cassingena A, Montone M, Bartolini A, Barault L, et al. Whole exome sequencing analysis of urine trans-renal tumour DNA in metastatic colorectal cancer patients. ESMO Open 2019;4:e000572.

69. Drost M, Tiersma Y, Glubb D, Kathe S, van Hees S, Calléja F, et al. Two integrated and highly predictive functional analysis-based procedures for the classification of MSH6 variants in Lynch syndrome. Genet Med 2020;22:847–56.

70. Seymour L, Bogaerts J, Perrone A, Ford R, Schwartz LH, Mandrekar S, et al. iRECIST: guidelines for response criteria for use in trials testing immunotherapeutics. Lancet Oncol 2017;18:e143–e52.

71. Von Hoff DD. There are no bad anticancer agents, only bad clinical trial designs–twenty-first Richard and Hinda Rosenthal Foundation Award Lecture. Clin Cancer Res 1998;4:1079–86.

72. Sartore-Bianchi A, Amatu A, Bonazzina E, Stabile S, Giannetta L, Cerea G, et al. Pooled analysis of clinical outcome of patients with chemorefractory metastatic colorectal cancer treated within phase I/II clinical studies based on individual biomarkers of susceptibility: a single-institution experience. Target Oncol 2017;12:525–33.

73. Kovalchik S, Mietlowski W. Statistical methods for a phase II oncology trial with a growth modulation index (GMI) endpoint. Contemp Clin Trials 2011;32:99–107.

74. Marcus L, Fashoyin-Aje LA, Donoghue M, Yuan M, Rodriguez L, Gallagher PS, et al. FDA approval summary: pembrolizumab for the treatment of tumor mutational burden-high solid tumors. Clin Cancer Res 2021;27:4685–9.

75. Vanpouille-Box C, Demaria S, Formenti SC, Galluzzi L. Cytosolic DNA sensing in organismal tumor control. Cancer Cell 2018;34: 361–78.

76. Lu C, Guan J, Lu S, Jin Q, Rousseau B, Lu T, et al. DNA sensing in mismatch repair-deficient tumor cells is essential for anti-tumor immunity. Cancer Cell 2021;39:96–108.

77. Mayer RJ, Van Cutsem E, Falcone A, Yoshino T, Garcia-Carbonero R, Mizunuma N, et al. Randomized trial of TAS-102 for refractory metastatic colorectal cancer. N Engl J Med 2015;372:1909–19.

78. Grothey A, Van Cutsem E, Sobrero A, Siena S, Falcone A, Ychou M, et al. Regorafenib monotherapy for previously treated metastatic colorectal cancer (CORRECT): an international, multicentre, randomised, placebo-controlled, phase 3 trial. Lancet 2013;381:303–12.

79. Morano F, Raimondi A, Pagani F, Lonardi S, Salvatore L, Cremolini C, et al. Temozolomide followed by combination with low-dose ipilimumab and nivolumab in patients with microsatellite-stable, O^6-methylguanine-DNA methyltransferase-silenced metastatic colorectal cancer: the MAYA trial. J Clin Oncol 2022;40:1562–73.

80. Yokota T. Are KRAS/BRAF mutations potent prognostic and/or predictive biomarkers in colorectal cancers? Anticancer Agents Med Chem 2012;12:163–71.

81. Tosi F, Magni E, Amatu A, Mauri G, Bencardino K, Truini M, et al. Effect of KRAS and BRAF mutations on survival of metastatic colorectal cancer after liver resection: a systematic review and meta-analysis. Clin Colorectal Cancer 2017;16:e153–e63.

82. Eisenhauer EA, Therasse P, Bogaerts J, Schwartz LH, Sargent D, Ford R, et al. New response evaluation criteria in solid tumours: revised RECIST guideline (version 1.1). Eur J Cancer 2009;45:228–47.

83. Li M, Chen WD, Papadopoulos N, Goodman SN, Bjerregaard NC, Laurberg S, et al. Sensitive digital quantification of DNA methylation in clinical samples. Nat Biotechnol 2009;27:858–63.

84. Barault L, Amatu A, Bleeker FE, Moutinho C, Falcomatà C, Fiano V, et al. Digital PCR quantification of MGMT methylation refines prediction of clinical benefit from alkylating agents in glioblastoma and metastatic colorectal cancer. Ann Oncol 2015;26:1994–9.

85. Medico E, Russo M, Picco G, Cancelliere C, Valtorta E, Corti G, et al. The molecular landscape of colorectal cancer cell lines unveils clinically actionable kinase targets. Nat Commun 2015;6:7002.

86. Chen L, Liu P, Evans TC, Ettwiller LM. DNA damage is a pervasive cause of sequencing errors, directly confounding variant identification. Science 2017;355:752–6.

87. Taylor AM, Shih J, Ha G, Gao GF, Zhang X, Berger AC, et al. Genomic and functional approaches to understanding cancer aneuploidy. Cancer Cell 2018;33:676–89.

88. Russo M, Crisafulli G, Sogari A, Reilly NM, Arena S, Lamba S, et al. Adaptive mutability of colorectal cancers in response to targeted therapies. Science 2019;366:1473–80.

89. Anagnostou V, Niknafs N, Marrone K, Bruhm DC, White JR, Naidoo J, et al. Multimodal genomic features predict outcome of immune checkpoint blockade in non-small-cell lung cancer. Nat Cancer 2020; 1:99–111.

90. Bergstrom EN, Huang MN, Mahto U, Barnes M, Stratton MR, Rozen SG, et al. SigProfilerMatrixGenerator: a tool for visualizing and exploring patterns of small mutational events. BMC Genomics 2019;20:685.

91. Díaz-Gay M, Vila-Casadesús M, Franch-Expósito S, Hernández-Illán E, Lozano JJ, Castellví-Bel S. Mutational Signatures in Cancer (MuSiCa): a web application to implement mutational signatures analysis in cancer samples. BMC Bioinf 2018;19:224.

92. Von Hoff DD, Stephenson JJ, Rosen P, Loesch DM, Borad MJ, Anthony S, et al. Pilot study using molecular profiling of patients' tumors to find potential targets and select treatments for their refractory cancers. J Clin Oncol 2010;28:4877–83.